1.0 INTRODUCTION AND LITERATURE SURVEY

1.1 Statement of the Problem

In many metallurgical processes such as the production of zinc, copper, manganese, nickel and cobalt, the mineral ore usually has metallic impurities, of which iron is the most common. Separating the iron from the mineral of interest is a common problem in these processes. In the production of manganese metal, iron is present as an oxide and may be removed by pyrometallurgical or hydrometallurgical means. The manganese metal produced hydrometallurgically usually has a higher purity than that produced pyrometallurgically.

The removal of iron by hydrometallurgical means is achieved by oxidising ferrous ions in a leach solution to the ferric state before precipitation by hydrolysis. From literature (Mathews and Robins, 1972; Dutrizac, 1986, etc.), the oxidation reaction process in a sulphate media is very slow without the use of a catalyst.

In this research work, it is attempted to remove iron as goethite from manganese leach liquor by oxidising ferrous sulphate to the ferric state at a controlled rate with air or oxygen. The research is aimed at achieving the following objectives:

- To establish experimental conditions such that is possible to selectively precipitate the iron from manganese in a sulphate solution
- To determine if impurities such as sulphates co-precipitate in the product. It is required to determine whether any intermediates are formed during the precipitation and possibly identify the species involved.
- To obtain a mathematical model that best describes the kinetics of the iron oxidation process.

1.2 Iron Removal From a Sulphate Solution

In a sulphuric acid leach, iron is commonly removed by oxidising it to the ferric state and precipitating Fe(III) by hydrolysis. The ferric ions in aqueous ferrous sulphate solution are generated by using oxygen as an oxidising agent (Dutrizac and Monhemius, 1986; Mathews and Robins, 1972; Vračar and Cerović, 1997).

The mechanism of the reaction has been investigated by many authors (Mathews and Robins, 1972; Huffman and Davidson, 1956; Vračar and Cerović, 1997; etc.). The general oxidation reaction of ferrous to ferric is given as:

$$4Fe^{2+} + O_2 + 4H^+ \rightarrow 4Fe^{3+} + 2H_2O \quad \ldots \quad (1.1)$$

The ferric ions are then precipitated out from solution using one of the following industrial processes (McAndrew *et al*, 1975; Dutrizac and Monhemius, 1986; Arslan, and Arslan, 2003).

1) *Goethite Process*

$$Fe^{3+} + 2H_2O \rightarrow FeOOH\ (s) + 3H^+ \quad \ldots \quad (1.2)$$

2) *Ferric Hydroxide Process*

$$Fe^{3+} + 3H_2O \rightarrow Fe(OH)_3\ (s) + 3H^+ \quad \ldots \quad (1.3)$$

3) *Hematite Process*

$$2Fe^{3+} + 3H_2O \rightarrow Fe_2O_3\ (s) + 6H^+ \quad \ldots \quad (1.4)$$

4) *Basic Ferric Sulphate Process*

$$Fe^{3+} + H_2O \rightarrow FeOHSO_4\ (s) + H^+ \quad \ldots \quad (1.5)$$

5) *Jarosite Process*

$$3Fe_2(SO_4)_3 + MeSO_4 + 12H_2O \rightarrow MeFe_6(SO_4)_4(OH)_{12}\ (s) + 6H_2SO_4 \quad \ldots \quad (1.6)$$

The following conditions are reported for each of the precipitation processes (Dutrizac and Monhemius, 1986; Scott and Davey, 1976).

Table 1.1 Industrial Processes for Iron Removal

Process	**Chemical Formula**	**pH**	**Temperature (^oC)**
Goethite	FeOOH	2 - 3.5	70 - 90
Jarosite	$MeFe_3(SO_4)_2(OH)_6$ Where Me = NH_4, K, H_3O, Na, Pb, etc	< 1.5	90 -120
Hematite	Fe_2O_3	Low acidity, Up to 2 % H_2SO_4	> 130
Ferric Sulphate	$FeOHSO_4$	High acidity > 2% H_2SO_4	> 130
Ferric hydroxide	$Fe(OH)_3$	~ 3	< 70

1.2.1 Iron Problem in Hydrometallurgical Manganese Circuits

In electrolytic manganese production, iron is removed from the leach solution to prevent serious problem in the purification procedures**.** Conventionally, in ores with low soluble iron content, the iron is usually removed from manganese

sulphate solutions by hydrolytic precipitation of ferric hydroxide ($Fe(OH)_3$) (Dutrizac and Monhemius, 1986; Hayes, 1993). Precipitating large quantity of this ferric hydroxide yields a massive unfilterable brown gel (Harris *et al*, 1977).

In the works reviewed above, the iron problem in manganese circuit has been attempted to be solved by trying to selectively precipitate the iron using goethite, jarosite and hematite processes. In the goethite process, iron is precipitated as an easily filterable crystalline goethite (Arslan and Arslan 2003). In all these processes, iron gels are therefore avoided (Hayes, 1993; Dutrizac and Monhemius, 1986).

1.2.2 eH – pH diagrams

The focus on this section is on the selection of thermodynamic conditions necessary for stability of iron, manganese and their products of hydrolysis. These are conveniently represented by Pourbaix diagrams (or E_h-pH diagram). The diagrams indicate the predominant species, present at equilibrium, given by reduction potentials and hydrogen ion concentrations (or pH). Also, the diagrams serve as an indication of the chemistry of the system at a particular temperature and set of activities of solute species.

Predominance Area Diagram for the Fe -Mn – H_2O system

In constructing the diagram, it is necessary to decide which species are to be considered and their energy of formation are listed as in Table 1.2.

Table 1.2 Thermodynamic data of species involved in Fe – H_2O systems

Species	**ΔG^o (298 K), kcal/mol**	**Reference**
Fe (s)	0.0	ARS
Fe^{2+}(aq)	-18.85	ARS
Fe^{3+}(aq)	-1.1	ARS
FeOOH(s)	-110.418	ARS
Fe_3O_4(s)	-242.7	ARS
H^+(aq)	0.0	LC
H_2O(aq)	-56.687	LC

ARS: Arslan and Arslan (2003); LC: Limpo and Cuadra (1977).

Using this data, a Pourbaix diagram is constructed for the iron species at 298 K as in Figure 1.1. The diagram is drawn for 10^{-3} M of all dissolved species present. A Sample calculation is given in Appendix A2.

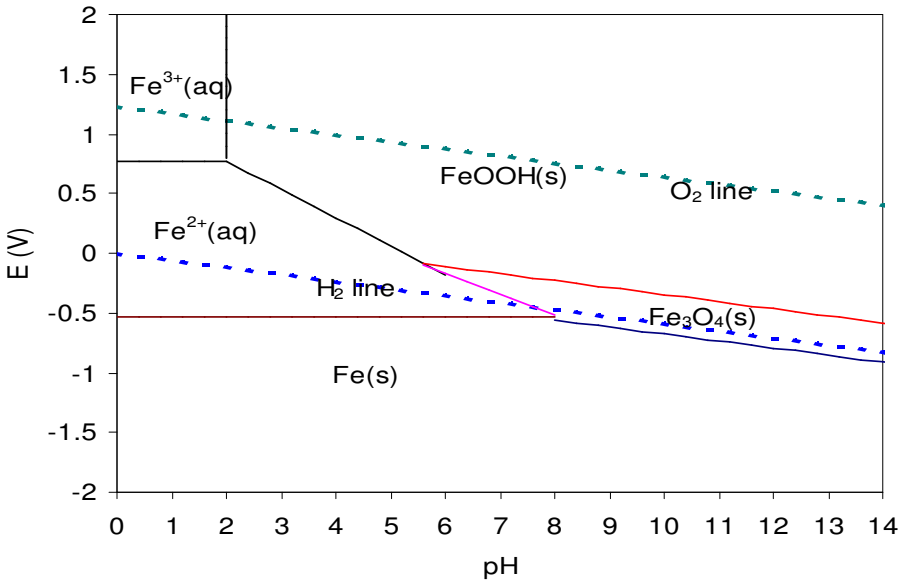

Figure 1.1 Eh – pH diagram of Fe –H_2O system at 298 K
Molarity of ionic species 10^{-3} M

Similar diagram is drawn for Mn – H_2O system at 298 K and presented as Figure 1.2.

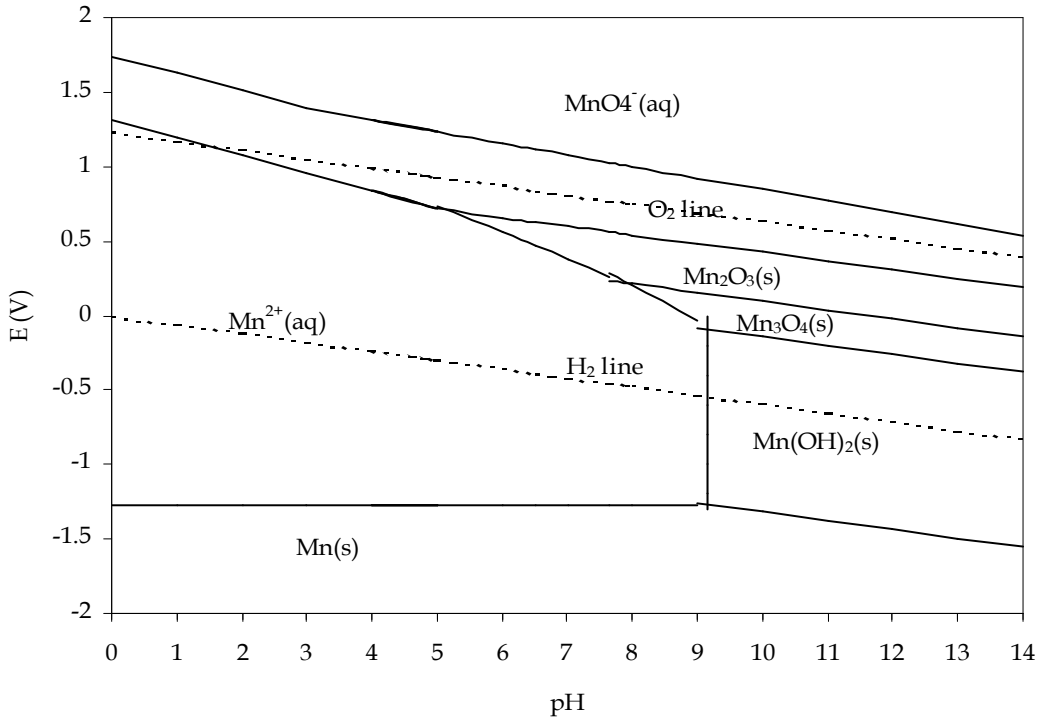

Figure 1.2 Eh – pH diagram of Mn –H_2O system at 298 K
Molarity of ionic species 10^{-3} M

From the two diagrams, the more acidic the solution is, the greater the stability region of the species of manganese and iron. From Figure 1.1, the goethite stability region is above the line where water is reduced to hydrogen. Therefore in order to precipitate iron as goethite from ferrous solution at 298K and 10^{-3} M ionic species, the solution needs oxidising.

The two diagrams are superimposed on each other to represent conditions where both iron and manganese ions are present in solution. This is illustrated in Figure 1.3. The 'operating region' in the diagram indicates that it is possible to selectively precipitate the iron as goethite and leave the manganese in solution.

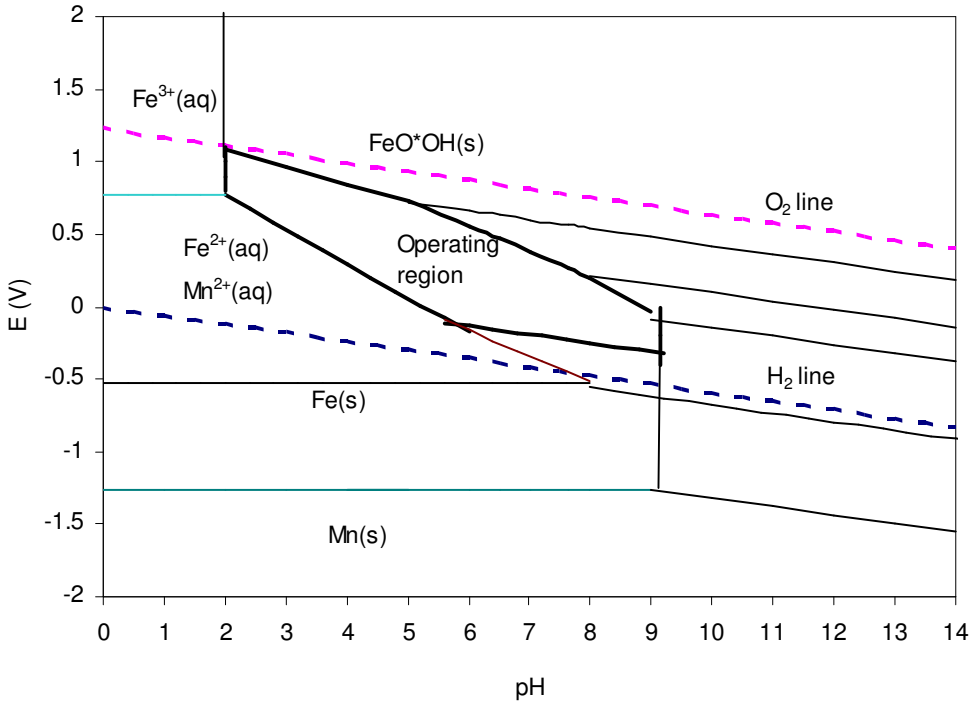

Figure 1.3 Eh – pH diagram of Fe – Mn – H_2O system at 298 K
Molarity of ionic species 0.001

1.2.3 Separation of iron in a form of goethite precipitate

The essential feature of the goethite process is to maintain the ferric concentration in the solution at no more than 1 g/l during precipitation (Scott and Davey, 1975; Burkin, 2001). This is achieved in the well-known processes of Vieille Montagne and Electrolytic Zinc. In Vieille Montagne process, all iron in the solution to be purified is reduced to the ferrous state and subsequently oxidised to ferric at a controlled rate with air (Scott and Davey, 1976). In the Electrolytic Zinc process on the other hand, ferric ion solutions are added to the precipitation vessel at a rate such that the soluble ferric ion does not exceed 1 g/l limit (Scott and Davey, 1976).

Scott and Davey (1975) performed laboratory scale experiments to study the two processes. They concluded that under their experimental conditions, the precipitate varied from well crystallised goethite (α - FeOOH) to poorly crystalline mixtures containing more of β – FeOOH in a sulphate media. They stated further that α - FeOOH was by no means the only product obtained during the precipitation of iron by the two processes.

Again, Scott and Davey (1976) established that better iron removal was achieved with Vieille Montagne procedure but product impurity levels were the same for both methods. According to them, appreciable contamination of the goethite by cation and anion impurities were evident. In sulphate systems the anionic contamination was due to some formation of basic sulphate.

In their attempt to separate iron completely from manganese sulphate solution, Sahoo *et al* (1978) performed experimental work using manganese ore (containing

28% manganese and 26% iron) obtained from Orissa, India. Their work indicated that at a lower pH of 3.5 very little iron was removed. At higher pH values, more iron was precipitated as ferric hydroxide, but manganese co-precipitated with the iron. They studied 'optimum' conditions where all the iron was removed and no manganese was lost to the solid.

Duby *et al* (1991) studied the kinetics of the goethite precipitation from sulphate solutions using an oxygen-sulphur dioxide mixture. According to them, the oxidation reaction proceeded very slowly when pure oxygen was used but accelerated significantly when sulphur dioxide or copper was added to the system. They established the presence of goethite in their solid analysis but mentioned that there was evidence of other compounds present as well. They neither made any attempt to determine what these compounds were nor formulate any mathematical model to describe their experimental conditions.

1.3 Oxidation of ferrous ions by dissolved oxygen

For the overall reaction of ferrous to ferric ions (Equation 1.1), Huffman and Davidson (1956) proposed that the reaction proceeded by simultaneous bimolecular and trimolecular reaction paths, for which the kinetic equation was described by:

$$r_{Fe(III)} = k_b [Fe(II)]\, p(O_2) + k_t [Fe(II)]^2\ p(O_2) \qquad \ldots \qquad (1.7)$$

where k_b and k_t are the reaction rate constants for the bimolecular and trimolecular reactions respectively. Studying the reaction at 140 – 180 ^oC, they observed a decrease in the reaction rate with increasing hydrogen ion concentration but did not incorporate this in their rate equation. They also mentioned the catalytic effect of Cu^{2+} ion on the reaction rate. Furthermore, they reported that the oxidation rate increased with increasing sulphate ion concentration (also not incorporated in rate equation), but the rate was independent of the hydrogen ion concentration in the range of 0.066 – 0.099M of Fe(II).

In their experiment where a gas lift percolator was used, Mathews and Robins (1972) proposed a rate equation of the form:

$$-r_{Fe^{2+}} = k_o \frac{[Fe^{2+}]^{1.84}[O_2]}{[H^+]^{0.25}} \cdot \exp(-\frac{73.9}{RT}) \qquad \ldots \qquad (1.8)$$

where k_o is the overall reaction rate constant. The ferrous concentration was measured spectrophotometrically and the H^+ concentration estimated from pH measurements at ambient temperatures. They determined the oxygen concentration from:

$$[O_2] = [O_2]_{sat} - \frac{k_m}{k_o} \qquad \ldots \qquad (1.9)$$

where k_m and k_o are the rate constants for the oxygen dissolution reaction and ferrous oxidation reaction respectively. The rate constant k_m was measured without any iron present in solution at the correct pH and temperature by measuring the dissolved oxygen concentration. No correction was made for the reduced solubility of oxygen as a result of other solutes present. The catalytic effect of the Cu^{2+} was confirmed in the work of Mathews and Robins (1972) where

they reported that the presence of the cupric sulphate increased the oxidation rate. Various salts such as $HgCl_2$, $ZnSO_4$, $CoSO_4$, Na_2SO_4 and MnO_2 were found to have negligible effect on the oxidation rate.

Studying the oxidation under oxygen pressure, Chmielewski and Charewicz (1984) presented second order kinetics with respect to [Fe(II)] and first order kinetics with respect to oxygen partial pressure with an activation energy of 56.9 kJ/mol K. This was reported for conditions where the ferrous ion concentration exceeded 3 – 8 g/l. They observed a deviation from the second order kinetics at lower ferrous concentrations and proposed that under these conditions the kinetics were first order with respect to the ferrous ion concentration. However, they did not quantify the kinetics of the ferrous ion at low concentrations since they were only interested in the technological importance at higher ferrous concentrations. They also confirmed the catalytic effect of the cupric ion on the oxidation.

Zhang *et al* (2000) confirmed the results by Chmielewski and Charewicz (1984) when they reported a second order rate with respect to the Fe^{2+} concentration.

Iwai, Majima and Awakura (1982) studied the oxidation of [Fe(II)] with dissolved molecular oxygen in sulphuric acid solutions using a glass autoclave. Again, they also proposed that the reaction occurs in two paths and presented a rate expression in the form:

$$-r_{Fe^{2+}} = A_O [Fe^{2+}]^2 \; p(O_2) \exp(-\frac{51.6}{R \cdot T}) + A_1 [SO_4{}^{2-})][Fe^{2+}]^2 \; p(O_2) \exp(-\frac{144.0}{R \cdot T}) \quad \ldots \quad (1.10)$$

They accounted for $FeSO_4$, $FeHSO_4^+$ and HSO_4^- species in the solution. Their work seemed to indicate that the role of the hydrogen ion is contradictory and made no

attempt to incorporate the hydrogen ion in their rate equation. Instead, they included sulphate ion in the rate equation and attributed some runs that deviated from second order kinetics with respect to [Fe (II)] to this ion.
Using an autoclave, Vračar and Cerović (1997) studied the oxidation reaction at elevated temperatures. They also reported that the reaction rate was second order with respect to Fe(II) concentration but limited by the diffusion rate of dissolved oxygen. An activation energy value of 51 kJ/mol was reported.

1.3.1 Reaction Mechanisms of Fe^{2+} oxidation with oxygen

It is evident from the above discussion that the oxidation of Fe^{2+} with O_2 has been widely studied for many systems, and in most cases, different mechanisms have been proposed.

In their literature review, Chmielewski and Charewicz (1984) mentioned that the oxidation rate in pure sulphate solution follows a second order expression with respect to the ferrous concentration. They confirmed this order at higher ferrous concentrations and mentioned that, at lower ferrous concentrations (< 0.143 mol/l) the rate is first order with respect to the ferrous ion, but did not suggest any mechanisms for the oxidation reaction.

Zhang *et al* (2000) reviewed the reaction sequence that described the mechanism for the oxidation of Fe^{2+} with oxygen as proposed by Weiss (1935). They presented the reaction sequence as:

$Fe^{2+} + O_2 \rightarrow Fe^{3+} + O_2^-$ Slow … (1.11)

$Fe^{2+} + O_2^- + 2H^+ \rightarrow Fe^{3+} + H_2O_2$ Fast … (1.12)

$Fe^{2+} + H_2O_2 \rightarrow Fe^{3+} + OH^{\cdot} + OH^-$ Fast … (1.13)

$Fe^{2+} + OH^{\cdot} \rightarrow Fe^{3+} + OH^-$ Fast … (1.14)

They further stated that the derived rate (Equation 1.15) from this reaction sequence is first order with respect to Fe^{2+} and only valid for oxidation under certain specific conditions like seawater, where the pH is in the range 6 to 8.

$$-r_{Fe^{2+}} = k[Fe^{2+}][O_2] \quad \text{...} \quad (1.15)$$

Mathews and Robins (1972) also proposed a reaction mechanism in sulphuric acid medium where the pH < 2. According to them, the mechanism for the reaction is by two parallel paths, and involves a ferrous – oxygen complex, FeO_2^{2+} with the following reaction sequence.

Path 1

$Fe^{2+} + O_2 \leftrightarrow Fe{\cdot}O_2^{2+}$ … (1.16)

$Fe{\cdot}O_2^{2+} + Fe^{2+} + H_2O \rightarrow 2Fe^{3+} + OH^- + HO_2^-$ … (1.17)

$HO_2^- + H^+ \rightarrow H_2O_2$ … (1.18)

$H_2O_2 \rightarrow H_2O + \frac{1}{2} O_2$ … (1.19)

Path 2

$Fe^{2+} + O_2 \leftrightarrow Fe{\cdot}O_2^{2+}$ … (1.16)

$Fe^{2+} + H_2O \leftrightarrow FeOH^+ + H^+$ … (1.20)

$Fe{\cdot}O_2^{2+} + FeOH^+ + H_2O \rightarrow 2Fe^{3+} + 5OH^-$ … (1.21)

They used the steady state approximation and derived rate equations for each rate path. For path 1, the derived rate equation is independent of hydrogen ion concentration

$$r_{[Fe^{3+}]} = \frac{k_{1.16}\, k_{1.17}\, [Fe^{2+}]^2 [O_2]}{k_{-1.16}} \qquad \ldots \qquad (1.22)$$

The rate equation for the second path was derived as

$$r_{[Fe^{3+}]} = \frac{k_{1.16}\, k_{1.20} k_{1.21}\, [Fe^{2+}]^2 [O_2]}{k_{-1.16}\, k_{1.21}\, [H^+]} \qquad \ldots \qquad (1.23)$$

Both paths indicate second order rate with respect to the ferrous concentration. The overall rate (Equation 1.24) was taken as the balance between the two paths.

$$r_{[Fe^{3+}]} = \frac{K[Fe^{2+}]^2 [O_2]}{[H]^{1/4}} \qquad \ldots \qquad (1.24)$$

The derived rate law from this mechanism agreed with their proposed empirical rate law.

Rönnholm *et al* (1999) proposed a similar rate law to that of Mathew and Robins (1972), but their mechanism for the non-catalytic oxidation of ferrous sulphate was 'assumed to proceed through the formation of an intermediate complex between dissolved oxygen and ferrous-ions and the cleavage of the O-O bond of the complex'. They presented their reaction steps as follows:

$$Fe^{II} + O_2 = (Fe\text{-}O\text{-}O)^{2+} \qquad \ldots \qquad (1.25)$$

$$(Fe\text{-}O\text{-}O)^{2+} + Fe^{II} = (Fe\text{-}O\text{-}O\text{-}Fe)^{4+} \qquad \ldots \qquad (1.26)$$

$$(Fe\text{-}O\text{-}O\text{-}Fe)^{4+} + Fe^{II} = (Fe_2\text{-}O)^{4+} + (O\text{-}Fe)^{2+} \qquad \ldots \qquad (1.27)$$

$(O\text{-}Fe)^{2+} + Fe^{II} = (Fe_2\text{-}O)^{4+}$ … (1.28)

$(Fe_2\text{-}O)^{4+} + H_3O^+ = OH^- + H_2O + Fe^{III}$ … (1.29)

$(H_3O)^+ + OH^- = 2H_2O$ … (1.30)

Overall reaction $4\,Fe^{II} + O_2 + H_3O^+ = 6H_2O + 4\,Fe^{III}$ … (1.31)

Assuming reactions 1.25 and 1.26 are the rate determining steps, they derived a rate expression based on these mechanisms (Appendix A5) in the form

$$r_{Fe^{II}} = \frac{\alpha[Fe^{II}]^2\, e^{-E/(RT)}[O_2]}{1+(\alpha/\beta)[Fe^{II}]} \quad \ldots \quad (1.32)$$

Where α and β are constants to be determined experimentally.

1.4 Theory on kinetics of iron oxidation

From the Pourbaix diagram (Fig.1.3), it is possible thermodynamically to selectively precipitate iron from manganese, but how fast is the precipitation? The selective precipitation experiments are conducted to answer this.

The oxidation of ferrous to ferric involves two processes, mass transfer of oxygen to reaction site and the oxidation of the ferrous ions. With reference to Figure 1.4, a hypothetical stagnant film is assumed to surround a gas bubble. It is assumed further that a linear concentration profile of oxygen exists within the film. The thickness of the film is δ and the concentration of oxygen is saturated at the

gas/liquid interface and equal to the bulk concentration at the outer edge of the film.

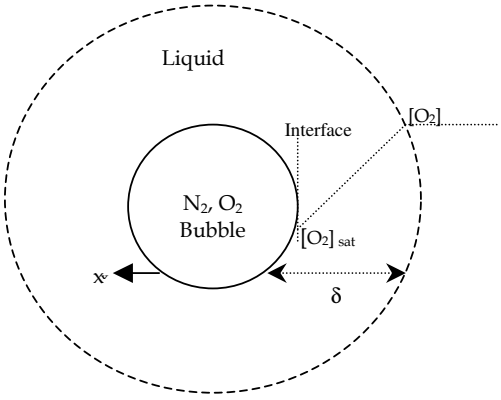

Fig. 1.4 Mass transfer of oxygen based on the ''stagnant film'' model

The rate of mass transfer of oxygen per unit reactor volume is given as:

$$\begin{aligned} r_{O_2} &= -D_{O_2}\, a_o \frac{d[O_2]}{dx}\Big|_{x=0} \\ &= -D_{O_2}\, a_o \frac{([O_2]-[O_2]_{sat})}{\delta} \\ &= \frac{D_{O_2}\, a_o}{\delta}([O_2]_{sat}-[O_2]) \\ &= k_m\, a_o\, ([O_2]_{sat}-[O_2]) \end{aligned} \qquad \ldots \qquad (1.33)$$

Where

$$k_m = \frac{D_{O_2}}{\delta} = Mass\ transfer\ coefficient$$

$$D_{O_2} = Molecular\ diffusivity\ of\ oxygen$$

$$a_o = Interfacial\ area\ of\ all\ bubbles\ per\ unit\ volume\ of\ aqueous\ phase$$

$$\delta = Apparent\ film\ thickness$$

A common feature of the rate models (Equations 1.7, 1.8, 1.15, 1.24, 1.32) is that

$$r_{Fe^{2+}} \ \alpha \ [O_2] \qquad \ldots \qquad (1.34)$$

More generally, $$-r_{Fe^{2+}} = -4\,r_{O_2} \qquad \ldots \qquad (1.35)$$

Meaning $$\frac{1}{4} r_{Fe^{2+}} = k'[O_2] \qquad \ldots \qquad (1.36)$$

Where k' is a lumped rate constant according to the rate models. I.e. all the parameters; k, [Fe (II)], [H^+] and exp (-E/RT) in the models are lumped together as k'.

Equating the two rates of oxygen, (1.33) and (1.36) and solving for oxygen concentration, [O_2].

$$[O_2] = \frac{[O_2]_{sat}}{1 + \dfrac{k'}{k_m a_o}} \qquad \ldots \qquad (1.37)$$

It is obvious that the concentration of oxygen is dependent on the mass – transfer coefficient and the saturated oxygen concentration in the solution.

Assuming chemical reaction is the controlling step, i.e. $k_m a_o >> k'$, then
[O_2] = $[O_2]_{sat}$, and the rate equations (1.7, 1.8, 1.15, 1.24, 1.32) can then be modelled in terms of the saturated oxygen concentration.

The saturated oxygen concentration is estimated from the empirical formula given by Narita *et al* (1983) in terms of partial pressure of oxygen, composition and temperature of the solution.

$$[O_2]_{sat} = 2.25 \times 10^{-3}\ p(O_2) \exp\left(\frac{1336}{T} - 4.48 - \sum K_i C_i\right) \qquad \ldots \qquad (1.37)$$

where C_i = concentration of i^{th} species

K_i = "solubility constant" for all ionic species and is given in Table 1.3

Table 1.3 Values of K_i

Species	K_i	Species	K_i
H^+	0.00	$NO3^-$	0.03
NH_4^+	0.08	Cl^-	0.07
K+	0.23	HSO_4^-	0.16
Na+	0.25	OH^-	0.19
Mg^{2+}	0.27	$SO4^{2-}$	0.28

In this dissertation, Mn^{2+} and Fe^{2+} are the interested species and are not listed above, therefore K_i value of 0.27 is assumed for each of these species.

2.0 EXPERIMENTAL

Type of solution used

A synthetic solution is used in all experiments because industrial leach solutions (leached ore) usually contain several impurities such as copper, cobalt and some alkaline metals, which may influence the oxidation reaction. E.g. alkaline metals may form jarosite compounds.

A manganese metal plant solution also contains ammonium sulphate as a buffering agent for the electrowinning cells. As the ammonium ion could form jarosite compounds, this salt is not added to the solution. In fact the composition of the synthetic solution used in this study is very similar to that which is encounted on an industrial electrolytic manganese dioxide (EMD) plant.

Chemicals

All reagents used are analytical grade. $FeSO_4.7H_2O$, $MnSO_4.H_2O$, MnO (E. Merck proanalysed) and sulphuric acid (BDH).

Gases in cylinders

Apart from the air, which is an instrument grade, all gases (oxygen and nitrogen) used are Ultra High Purity (UHP) supplied by Afrox. The cylinders containing the gases are fitted with pressure regulators and connected to the reactor through 1/8-inch copper tubing. The line pressure is maintained at approximately 1.5 bar. All the lines are fitted with needle valves that handle flow rate up to 5 l/min. The lines are joined to a common flowmeter (rotameter) that monitors the gas flowrate.

From this, the gas is introduced into the reactor through rubber tubing and a gas sparger as shown in Figure 2.3.

Rotameter

The rotameter used is self-made and could handle the required gas flowrate of 2.0 l/min. The instrument is calibrated, by using a soap bubble meter. The calibration curve is shown as Figure 2.1.

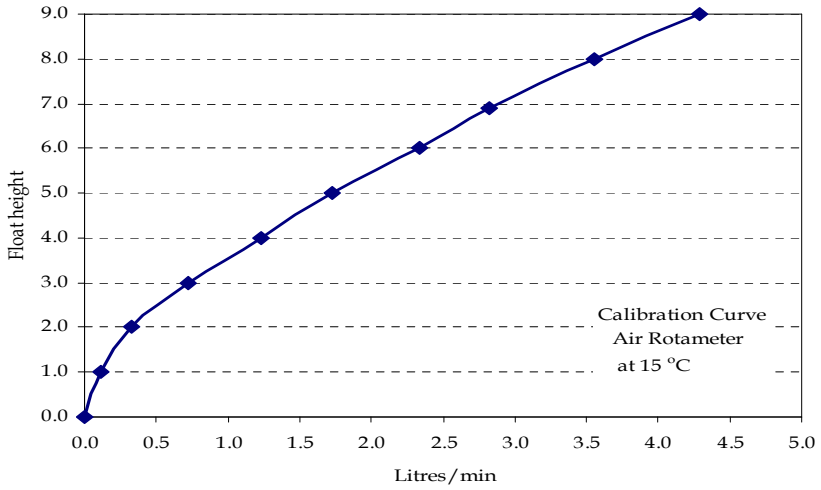

Figure 2.1 Calibration curve for air rotameter

Other equipment

Cresson pH probe and Cyberscan pH metre are used to monitor the reaction pH. An E_h probe using Pt working electrode and Ag/AgCl reference electrode is used to monitor solution potential.

The temperature in the reactor is automatically controlled by an on/off switch connected to a hotplate as shown in Figure 2.2.

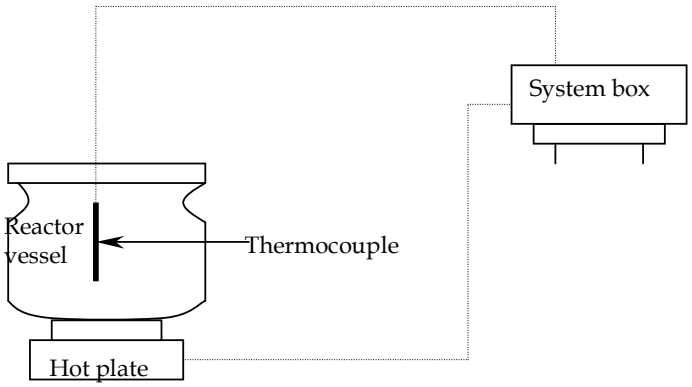

Figure. 2.2 Temperature Control Set-up

2.1 Experimental Set-up

The setup for the experiment is shown as Figure 2.3. The experiment is operated batchwise with respect to the liquid phase. The gas (oxygen, nitrogen or air) is introduced into the reactor through 1/8 inch copper tubing controlled by a needle valve and monitored by a rotameter. A 4 *l* cylindrical glass vessel (with flat bottom) is used as the reactor. The vessel lid is fitted with 6 ports that houses a stirrer, pH and temperature probes, condenser, thermocouple and a gas sparger. The sixth port is used for sampling. The reactor is heated on a hotplate, which is connected to a temperature controller. The gas sparger disperses the gas in the form of small bubbles. Due to the large amount of water vapour that is released during the reaction, a condenser large enough to condense most of the vapour is used.

2.2 Experimental Procedure

Before the experiment commenced, distilled water is de-oxygenated by bubbling ultra pure nitrogen through 25 *l* of the water overnight. Solution containing ferrous sulphate ($FeSO_4.7H_2O$) and manganeous sulphate ($MnSO_4.H_2O$) is prepared by weighing appropriate amounts of their solids into the reactor. 2.75 *l* of de-oxygenated water is then added to make up the solution. For all experiments, 32 g/l of Mn^{2+} concentration is used. The reactor lid is fitted, all ports sealed with stoppers and the overhead stirrer fitted. The reactor and its content are then placed on the hotplate; the stirrer is turned on at low speed to dissolve all the solids.

Once the solids are dissolved, the hotplate is switched on and the appropriate temperature is entered into the system box. All stoppers are then removed and fitted with condenser, pH / temperature probe, thermocouple and gas sparger. The stirrer speed is then increased to 240 rpm and the solution is allowed to reach the required temperature. While heating, nitrogen gas is bubbled through the solution at approximately 1.0 l/min to avoid any oxidation of ferrous constituents. To adjust the pH to above 6, solid MnO is added. Other common neutralizing agents are unsatisfactory in the sulphate media as alkali metal hydroxides and ammonia encourage the formation of jarosites, and calcium carbonate could form insoluble calcium sulphate. The solution is left further for about 2 hours to completely dissolve all the solids. When a pH of about 6.0 is reached, nitrogen gas is turned off and replaced with oxygen. The gas flowrate is maintained at 2.0 l/min (a flow rate which is set by the needle valves). The solution pH is then monitored as a function of time. Similarly, total iron and manganese concentrations are monitored by taking samples at appropriate times.

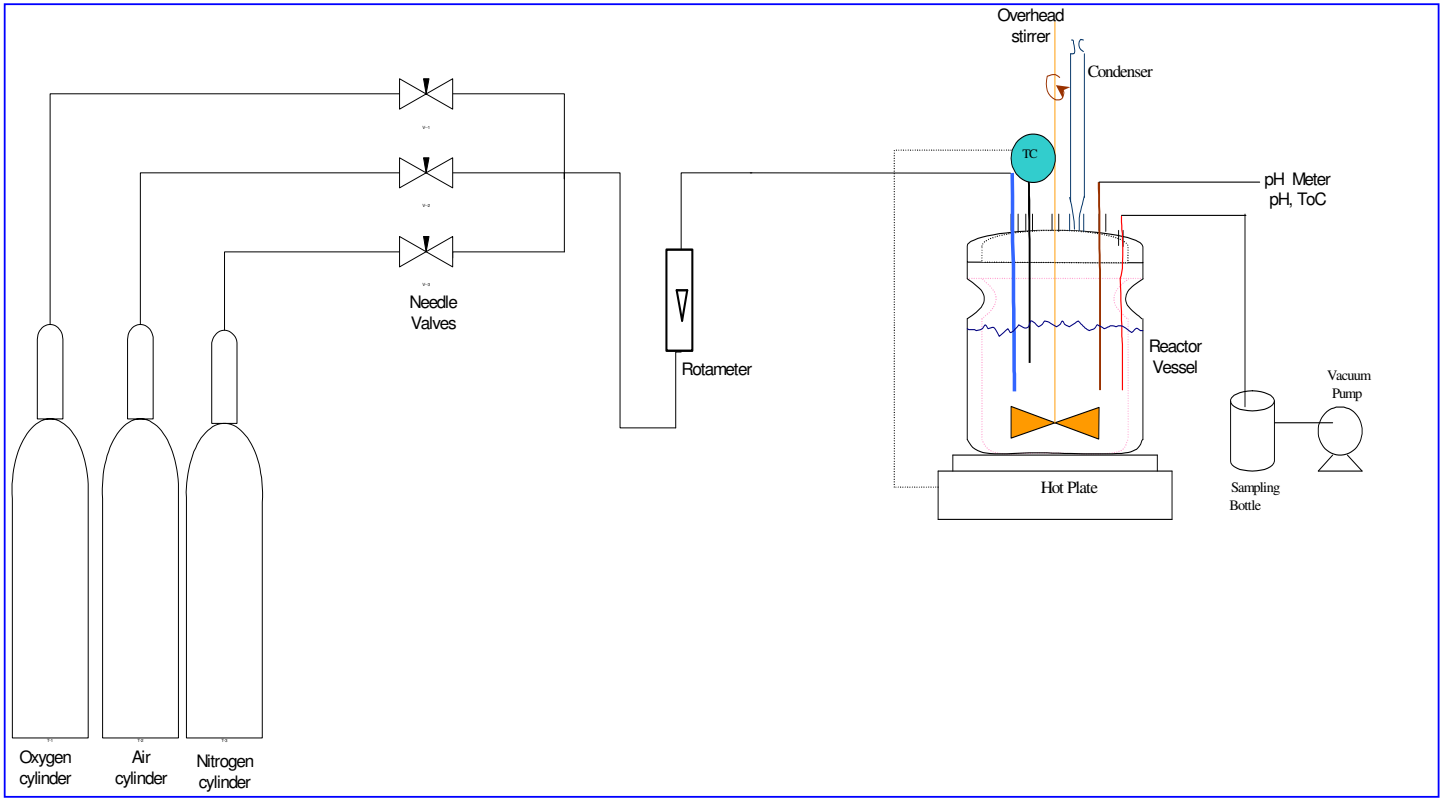

Figure 2.3 Experimental Set-ups

2.3 Filtration system

Samples are drawn from the reactor by a vacuum filtration system as shown below in Figure 2.4. This is done to avoid any introduction of air when sampling. In this set-up, a Millipore filter paper with pore size of 0.22 μm is placed in a 55 mm (ID) Buchner funnel. The funnel is closed at the top to create a vacuum. This is fitted to a sample bottle. A valve is connected to ensure that approximately 10 ml of a sample is drawn at each time interval.

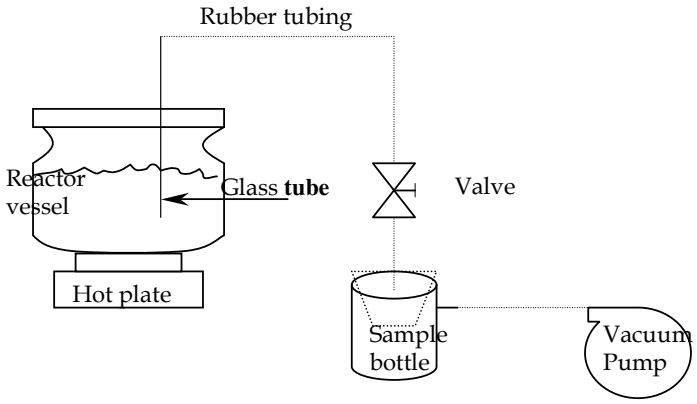

Figure. 2.4 Filtration system

At each sample time, the vacuum pump is switched on and the valve is opened slightly to draw the sample. Once an appropriate amount is drawn, the vacuum pump is switched off. The samples are filtered automatically. Solid samples are washed through with 50 ml distilled water, dried in an oven at 55 ^{o}C overnight and stored for further analysis. A drop of sulphuric acid is added to the liquid samples to avoid further oxidation by air and are then analysed by Atomic Absorption Spectrometer (AAS) for total iron and manganese concentrations.

2.4 Preliminary results

Preliminary experiments showed that in order to dissolve the MnO to obtain as high a starting pH as possible, it was necessary to introduce baffles into the glass vessel. Four baffles are made from grey Teflon and held in position in the reactor by applying silicon black and left for 24 hours to dry. After this, the pH could be raised to 6 and almost all the MnO added is dissolved after about two hours. In some instances, small amounts of the solids still remained after the first sample is taken, but are thought to be small enough to ignore. The baffles also help to eliminate mass transfer effects (due to poor mixing) in the reactor.

2.5 Experiments conducted

In order to achieve the objectives outlined earlier in the introductory section, parameters such as temperature, starting ferrous concentration and type of oxidising media (air or oxygen in this case) are considered in the experimental work. Systematic experiments are carried out at initial ferrous concentration and temperature ranges between 5 – 20 g/l and 55 – 85 ^{o}C respectively.

3.0 RESULTS AND DISCUSSIONS

3.1 Confirmation that mass transfer effects can be neglected

Increasing the oxygen flowrate from 2.0 l/min to 3.5 l/min has little effect on the oxidation rate (Figure 3.1). Similar hydrogen ion concentration is released into the solution. Therefore the flowrate is fixed at 2.0 l/min.

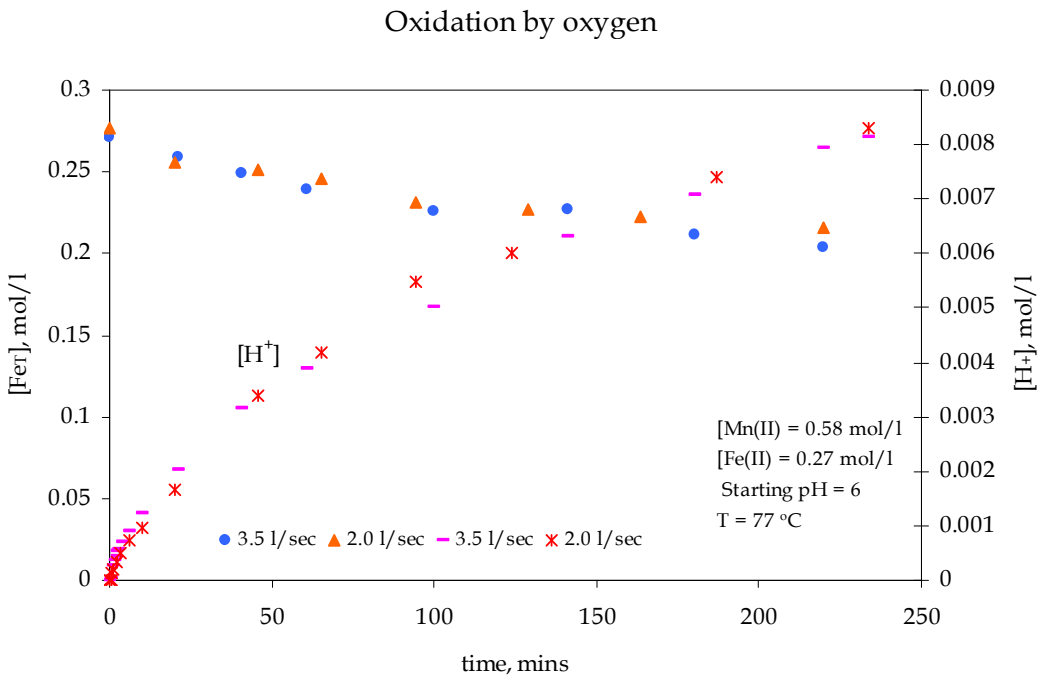

Figure 3.1 Effect of flowrate on oxidation rate

Similarly, decreasing the stirrer speed from 240 rpm to 200 rpm has little effect on the oxidation rate (Fig. 3.2). The stirrer speed is fixed at 240 rpm for the remainder of the experiments.

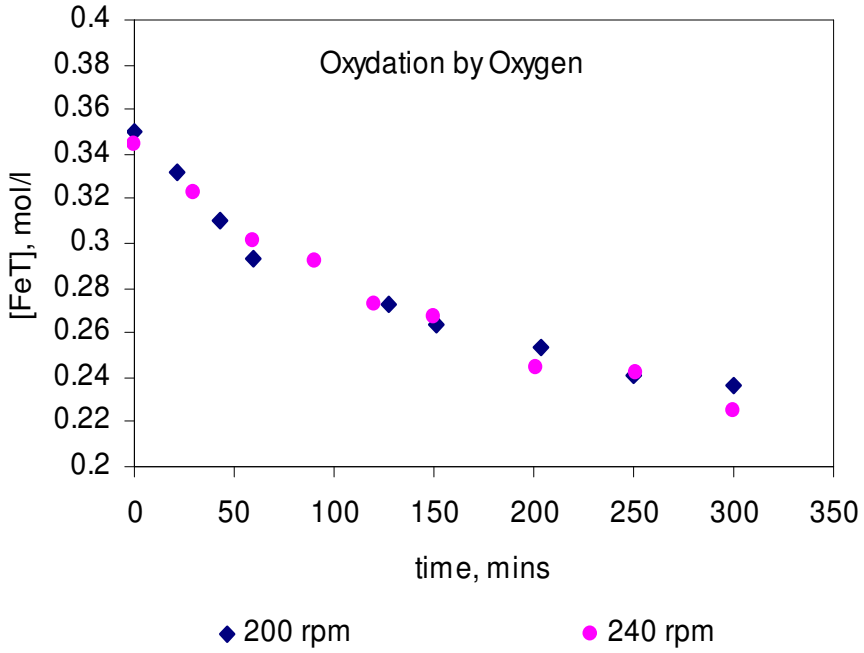

Figure 3.2 Effect of stirrer speed on oxidation rate

3.2 Reproducibility of experimental results

Three separate runs are performed with a starting ferrous concentration of 0.176 mol/l using oxygen. All other conditions are the same and the results are illustrated in Figure 3.3.

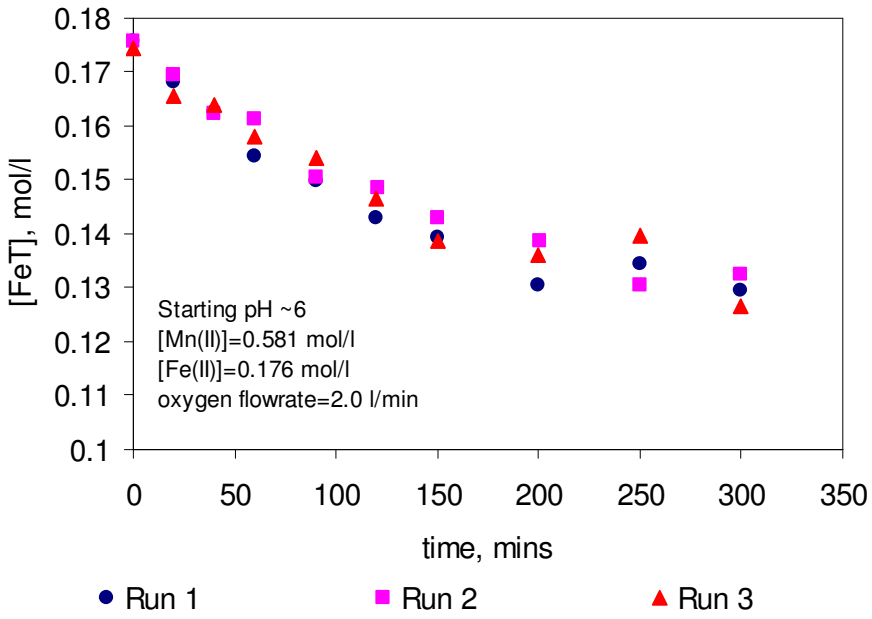

Figure 3.3 Testing for reproducibility of experimental runs

From these results it is concluded that the runs are sufficiently reproducible.

3.3 Determination of Solids Composition

3.3.1 Solution Phase Analysis

Using AAS, the concentrations of manganese are monitored as functions of time (Fig. 3.4) to determine if manganese co-precipitated with the iron (as discussed by Sahoo *et al,* 1978). Figures 3.4a and b are the analyses for high and low initial ferrous concentrations. The graphs are an indication of the selective precipitation of the iron from the manganese based on the analysis of the aqueous solution. The two Figures show the loss of iron into the solid phase while manganese still remains in solution at a relatively steady concentration. Similar analyses are made for each run conducted so that any co-precipitation could be identified. All showed no sign of co-precipitation of manganese with the iron.

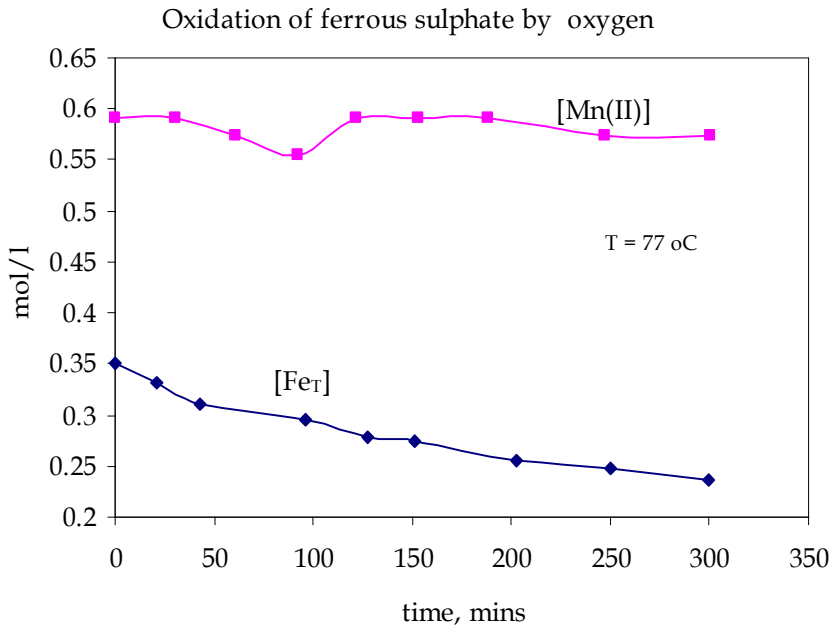

Figure 3.4a Evidence of selective precipitation of the iron from manganese

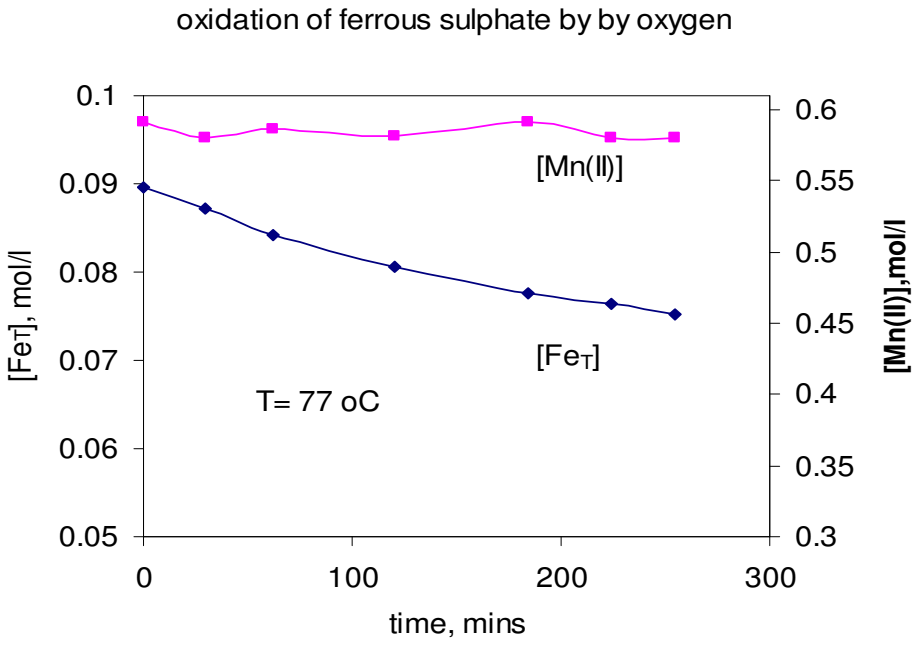

Figure 3.4b Evidence of selective precipitation of the iron from manganese

3.3.2 Solid Phase Analysis

The selective precipitation of the iron is confirmed even further by conducting additional experiments. These experiments are conducted for specific times without any intermediate samples taken. After the conclusion of each run, the content of the reactor is filtered in a Buchner funnel and the solids are washed with approximately 500 ml distilled water. The filtered solids are dried in an oven at 55 ^{o}C and left overnight. Manganese and iron are determined on the AAS by dissolving in HCl solution and sulphate is analysed gravimetrically using barium sulphate (See Appendix A4). The analyses of the solids are presented in Table 3.1.

Unless stated otherwise, all experiments are conducted at 77 °C with oxygen and have MnO added to raise the pH. Water content is determined by heating the solids in an oven at 600 °C. Only selected starting ferrous concentrations are analysed for H_2O and sulphate species with the idea of identifying any possible trends that might develop.

Table 3.1 Solids analyses

Expt. No.	Starting [Fe(II)] mol/l	Run time, minutes	Fe Content % (mass)	Mn Content % (mass)	SO_4 Content % (mass)	H_2O Content % (mass)
R1	0.032	60	72.0	0.78	4.98	-
R2	0.089	60	69.8	1.04	5.75	-
R3[T]	0.089	420	64.3	1.14	-	-
R4	0.171	60	68.3	1.23	4.92	-
R5	0.171	200	66.0	1.19	-	-
R6	0.351	60	62.8	1.20	8.34	-
R7	0.351	200	62.7	1.11	8.23	25.1
R8[W]	0.351	200	63.1	1.19	3.47	-
R9*	0.351	200	63.3	1.24	8.67	24.8

[T] Experiment conducted at 55 °C
[W] Solids washed through again with distilled water
* Experiment conducted without the addition of MnO

It is clearly evident from the manganese content in the solids that, limited manganese co-precipitates with the iron. This indicates that at the selected experimental conditions, it is possible to almost completely separate iron from

manganese, which agrees with literature (Sahoo *et al*, 1978). It is necessary however to investigate if the small amount of manganese content is as a result of slight co-precipitation with the iron, or because of incomplete dissolution of the solid MnO (added to the solution to raise the reaction pH). In order to prove this, experiment R9 in Table 3.1 is performed without any solid MnO added. It is evident that almost similar amounts of manganese are present in the solids. Hence, it is concluded that small amount of manganese do co-precipitates with the iron.

The sulphate analysis in Table 3.1 is done to get an indication of the type of basic sulphate species formed with or as intermediate in the goethite precipitation as mentioned by some authors (Scott and Davey, 1976; Duby *et al*, 1991). Starting with high ferrous concentrations, the runs are done for a period of 60 and 200 minutes to establish when the basic sulphate actually formed. All the iron compounds given in Table 1.1 are possible products of the reaction. The theoretical iron and sulphates contents that would be present if iron is precipitated as any of the iron compounds is given as Table 3.2.

Table 3.2 Theoretical contents of species present in solid precipitates

Compound	Fe cont. % (by mass)	SO_4 cont. % (by mass)
$Fe(OH)_3$	52.3	-
Fe OO H	62.9	-
Fe OH SO_4	33.1	56.9
$H_3O\ Fe_3(SO_4)_2(OH)_6$	34.9	40.0

The experimental sulphate contents present in the solids (Table 3.1) are far lower than expected theoretically (Table 3.2). Based on this and the iron content

reported experimentally (Table 3.1), it is assumed that the precipitate compound likely to form is goethite (Fe OO H).

To prove that the sulphate contents in the solids are not as result of poor washing of the precipitates, the solids of experiment R7 are washed a second time with distilled water and presented as experiment R8 in Table 3.1. The solid precipitate is again dried overnight at 55 ^{o}C and analysed. It is clear from the sulphate analysis of R8 that more than half of the sulphate content (of R7) present in the solids is due to poor washing of the solids. Nonetheless, a small amount of the sulphate is still present in the solids presumably as result of precipitation.

3.3.3 TGA Analysis of the solids

In order to establish whether the precipitate is of an anhydrous nature, thermal gravimetric analysis (TGA) is done on some solid samples. Figure 3.5 shows the percent weight loss of the solids as a function of temperature for a heating rate of 10 ^{o}C/min. The analyses are done for higher starting ferrous concentrations (R7 and R9). The weight loss can be seen to happen at two different temperatures (around 200 ^{o}C and 600 ^{o}C). The early and the late water loss is an indicative of formation of goethite compound. A view, which is supported by the large water loss, which continues up to 200 ^{o}C. The results are in agreement with literature Scott and Davey (1975). Also, both graphs display similar total water loss by the TGA, confirming the total water content that is reported in Table 3.1 when the solids are heated in oven at 600 ^{o}C.

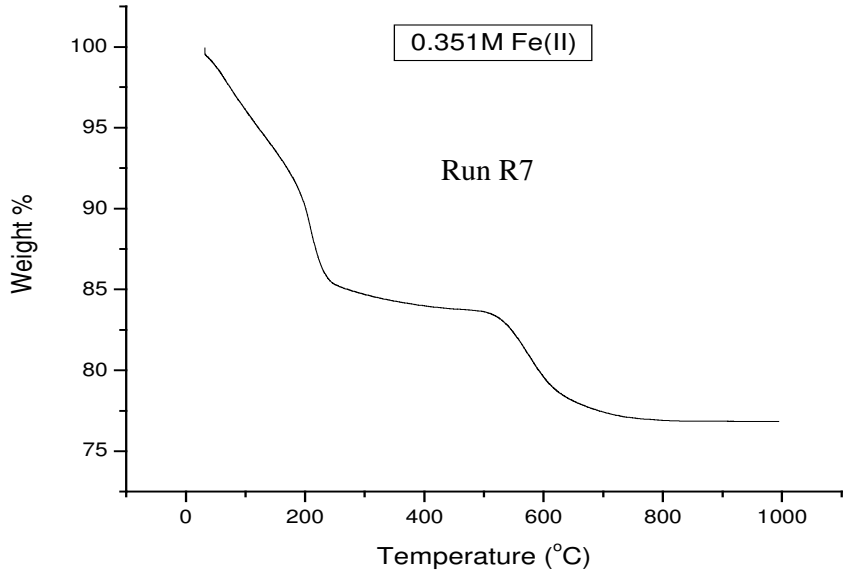

Figure 3.5a TGA analysis of solids

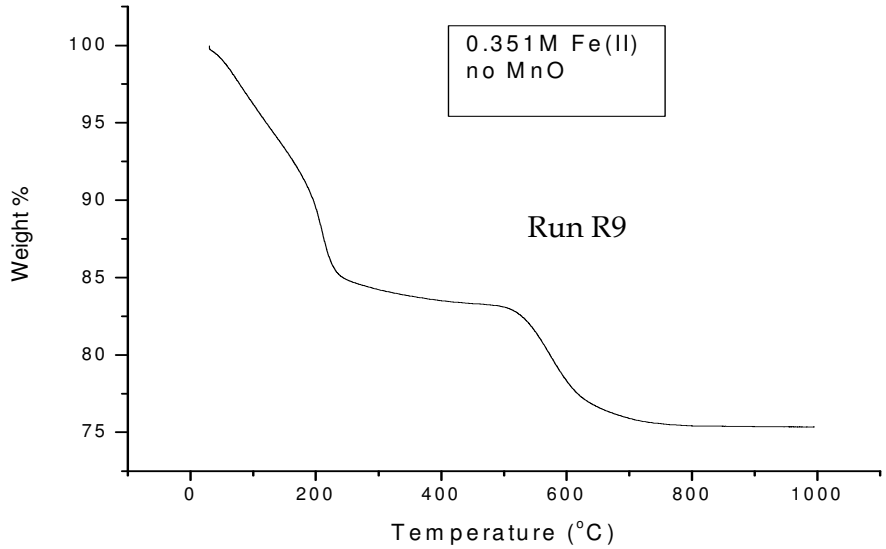

Figure 3.5b TGA analysis of solids (no MnO added to the solution)

3.3.4 XRD Analysis of the solids

An XRD analysis is done on the solid samples to have an indication of the precipitate compound(s) formed (Figure 3.6).

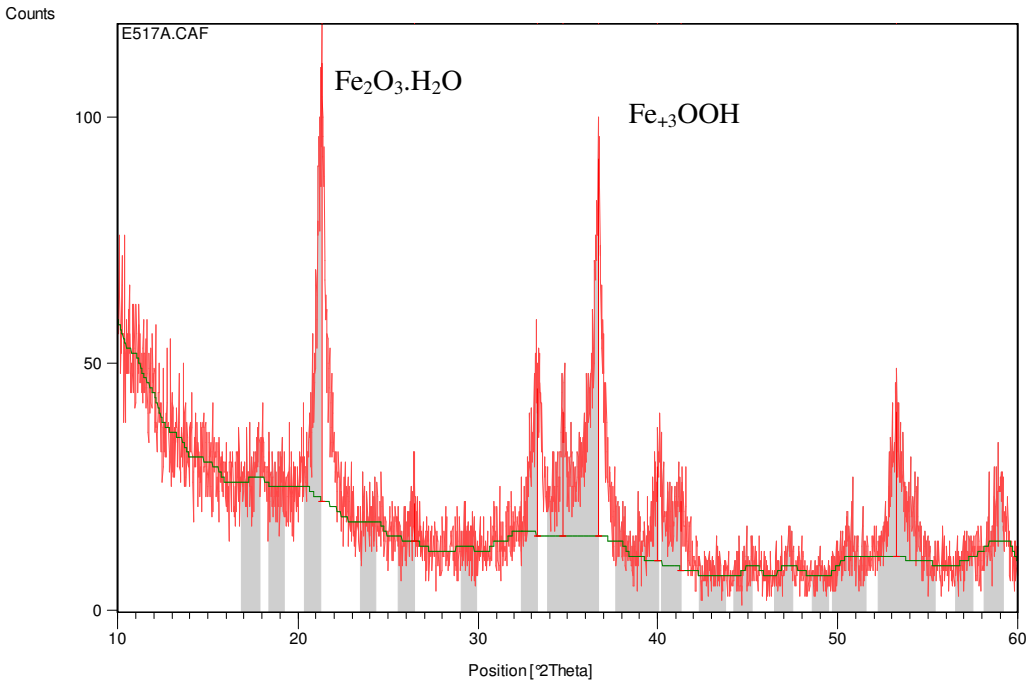

Figure 3.6 XRD analysis of the solid sample

The analyses obtained from the XRD and TGA confirm goethite is the main precipitate compound formed in the oxidation reaction. Traces of manganese and sulphate compounds are also present. The results are in agreement with literature (Scott and Davey, 1975,1976; Duby *et al*, 1991).

From Table 3.1, the mass balance is shown to account up to about 97%. The remainder can possibly be attributed to some errors in the analysis (AAS and

gravimetric). For an example, approximately 8.5% error is calculated for the gravimetric analysis of the sulphate content (Appendix A4).

3.4 Effect of parameters on oxidation rate

3.4.1 Effect of Initial ferrous concentration

Figure 3.7 shows the normalised rate curves for the oxidation reaction by molecular oxygen at different starting ferrous concentrations. The rates are very small particularly at low initial ferrous concentration. Further rate curves are presented in Appendix A3. The results are consistent with data in the literature (Duby *et al*, 1991; Zhang *et al*, 2000; Iwai *et al*, 1982).

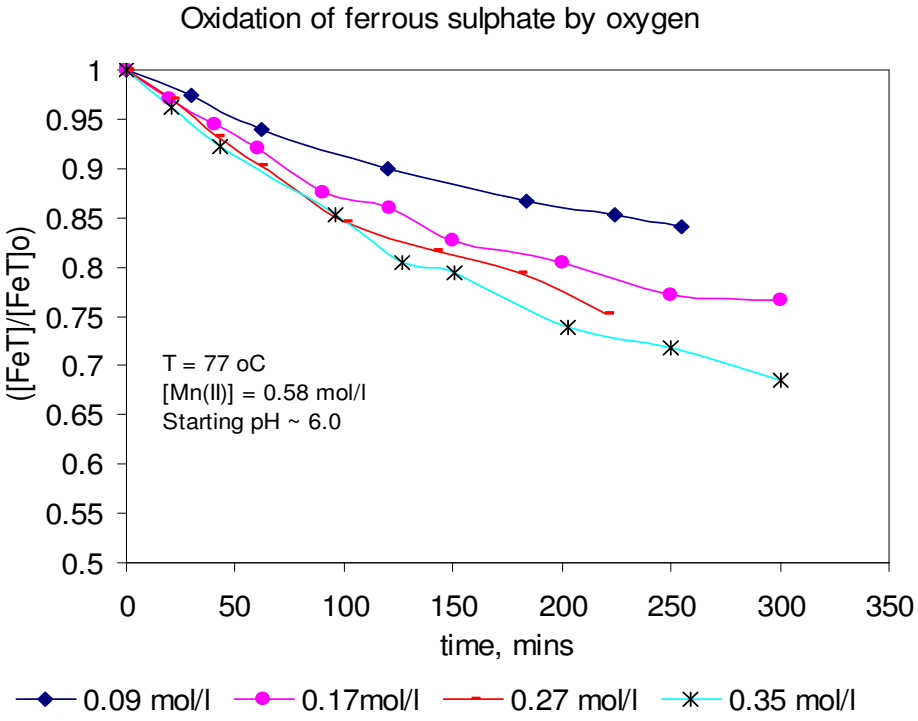

Figure 3.7 Effect of starting [Fe (II)] on the oxidation reaction

3.4.2 Effect of oxidant type

The effect of oxidant type is presented in Figure 3.8. The Figure shows the rate curves for two different starting ferrous concentrations. It is evident from the graphs that only a small amount of precipitation took place when air is used.

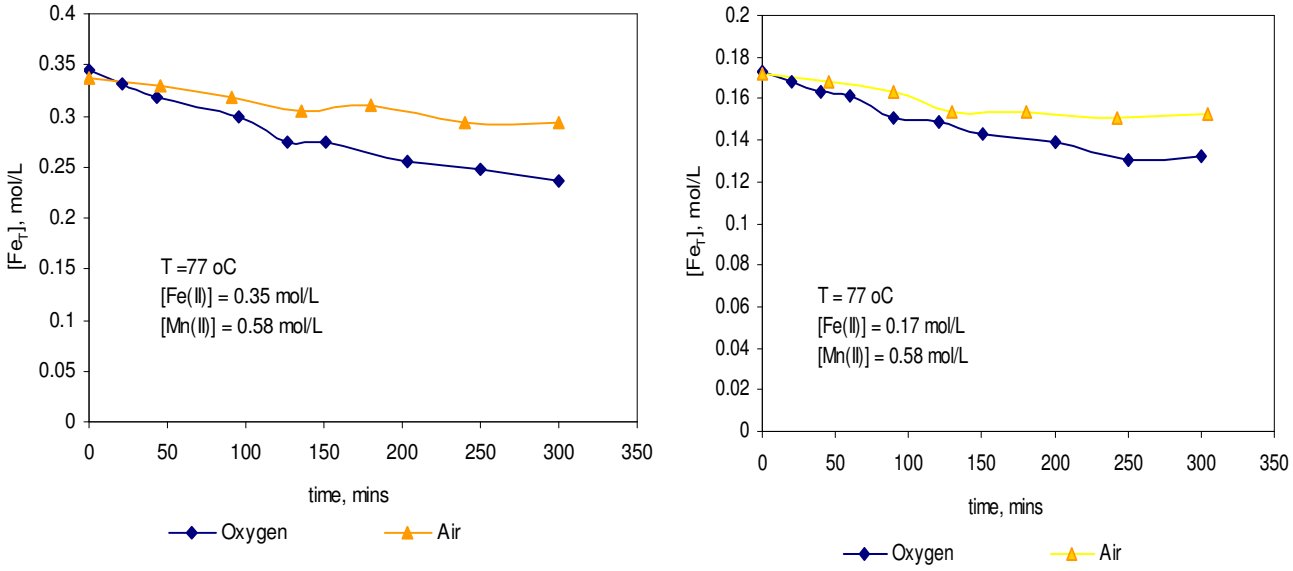

Figure 3.8 Effect of different oxidant on the oxidation process

3.4.3 Effect of temperature

Figure 3.9 shows the temperature effect on the oxidation reaction. The temperature effect is investigated using the highest ferrous concentration.

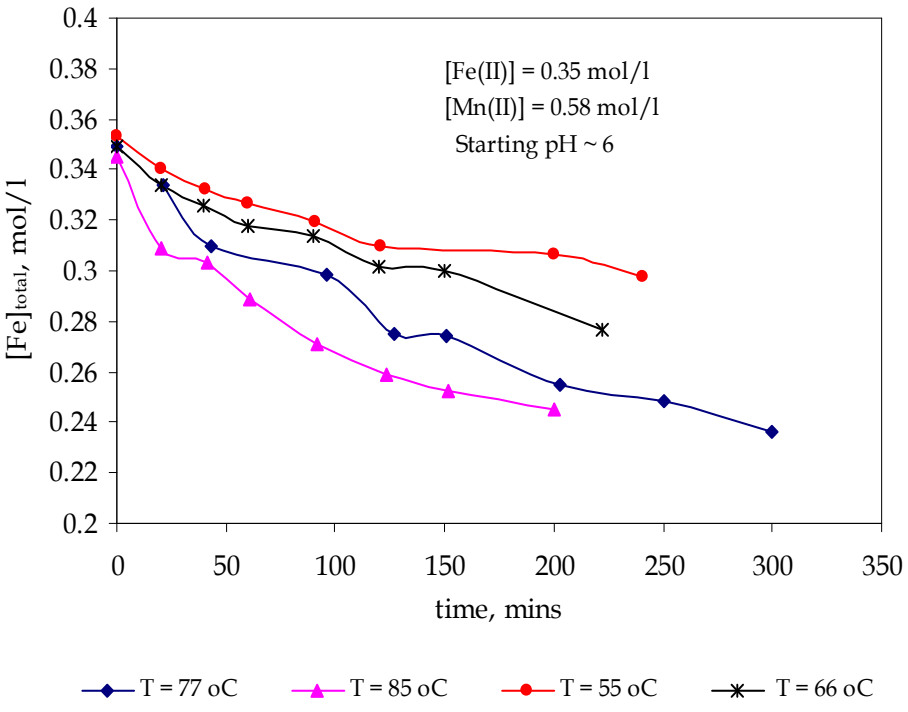

Figure 3.9 Effect of temperature on the oxidation rate

The rate increases with temperature and is consistent with literature (Mathews and Robins, 1972; Vračer and Cerović, 1997; Chmielewski and Charewicz, 1983).

3.4.4 Effect of pH

The control of the reaction pH proved to be difficult; therefore the oxidation process is performed at as high pH values as possible to effect appreciable reaction rates.

Using oxygen, an experiment is conducted at low pH value (3.5) to investigate the significance of the low pH on the reaction rate. The low pH run has no MnO added to the solution. The results are shown in Figures 3.10 and 3.11.

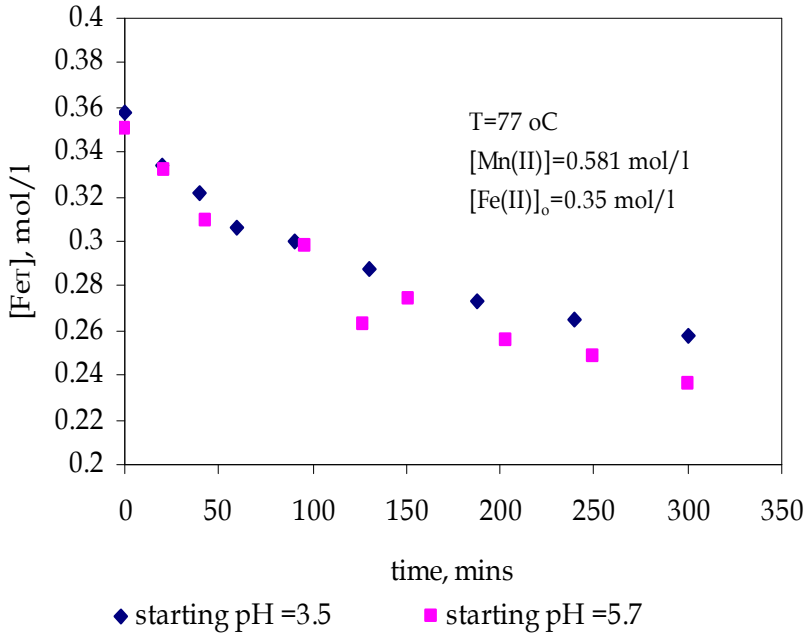

Figure 3.10 Effect of starting pH on the oxidation rate

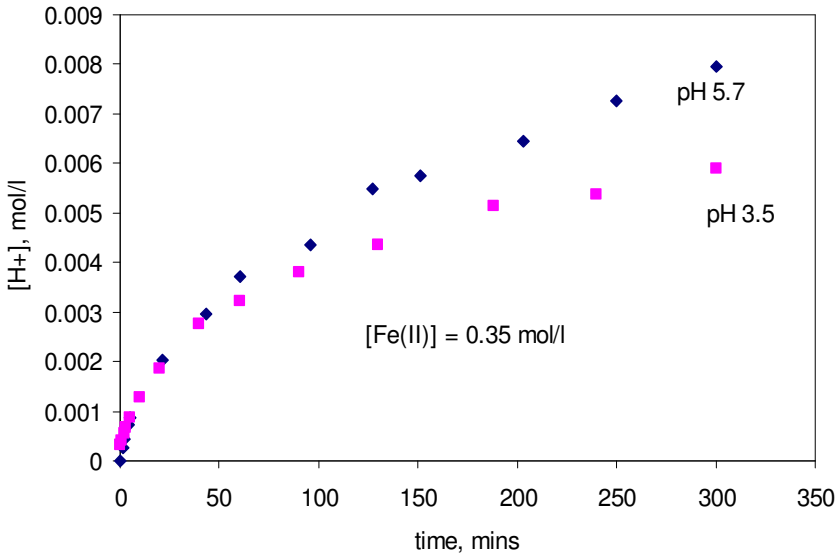

Figure 3.11 The release of $[H^+]$ in the oxidation reaction

It is evident from the graphs that the starting pH has only small effect on the oxidation rate. This is in general agreement with literature (Iwai *et al,* 1982).

3.4.5 eH-pH diagram

Figure 3.12 shows the measured solution potential as a function of pH using silver silver-chloride reference electrode for the high initial ferrous concentration (Run R7).

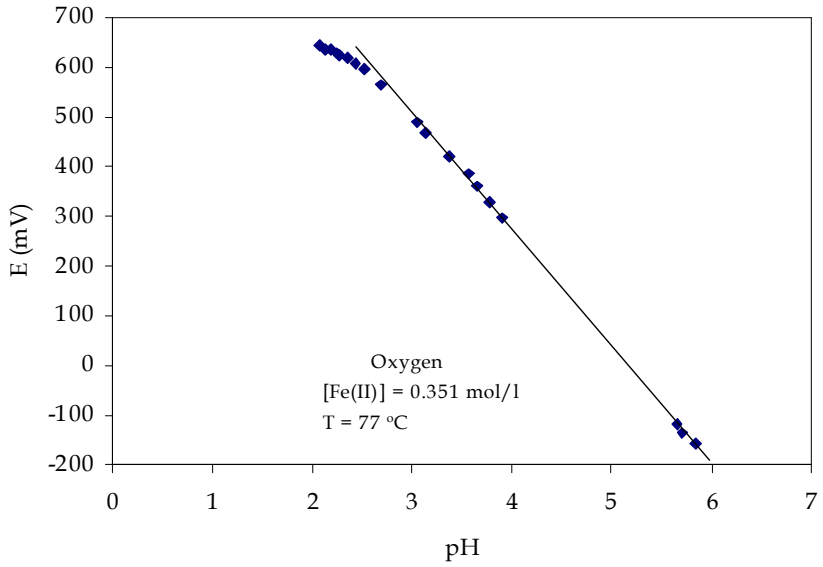

Figure 3.12 eH-pH diagram of reaction solution

The equilibrium potential for the precipitation of iron is governed by the ferric to ferrous species (Hayes, 1993) according to equation 3.1

$$Fe^{3+} + e = Fe^{2+} \quad \ldots \quad (3.1)$$

For the half reaction, the Nernst Equation is applied

$$E_h = E_o - \frac{RT}{n\,F} \ln\left(\frac{a_{red}}{a_{oxd}}\right) \quad \ldots \quad (3.2)$$

And in terms of concentrations

$$E_h = E_o - \frac{RT}{n\,F}\ln\left(\frac{[Fe^{3+}]}{[Fe^{2+}]}\right) \quad \ldots \quad (3.3)$$

Now, let $E_h' = E_h - E_o$ and constant depending on temperature, C = RT/n F. From the earlier discussion, goethite is the main solid species that is formed in the reaction.

$$Fe^{3+} + 2H_2O = Fe\,OOH\,(s) + 3H^+ \quad K_1 \quad \ldots \quad (3.4)$$

If it is assumed that the solids are in equilibrium with the ferric species, then

$$[Fe^{3+}] = [Fe\,(OOH)\,]\,[H+]^3 \,/\, K_1 \quad \ldots \quad (3.5)$$

Substituting this into Eq. 3.3 and rearranging

$$E_h' = \ln\left(\frac{[FeOOH]}{K_1[Fe^{2+}]}\right)C + 3C\ln[H^+] \quad \ldots \quad (3.6)$$

The terms in the bracket are assumed to be constant. For R = 8.314 J/mol K, F = 96487 J/mol V and T = 350K, C = 0.03; equation 3.6 becomes

$$E_h' = const + (-0.201\,pH) \quad \ldots \quad (3.7)$$

This is a straight-line equation (E_h' vs. pH) of slope –0.201. From the graph of Fig. 3.12, the slope of the straight line is approximately –0.23. This confirms that the solids are in equilibrium with the ferrous ion, which is also in equilibrium with the hydrogen ion concentration.

Ferrous and ferric species

Using the highest ferrous concentration, the ratio of ferric to ferrous (Fe^{3+} / Fe^{2+}) is calculated for the reaction pH range (Figure 3.13). Clearly, the ferric ion in the solution is negligible, therefore it is plausible to assume that [Fe (III)] ~0.

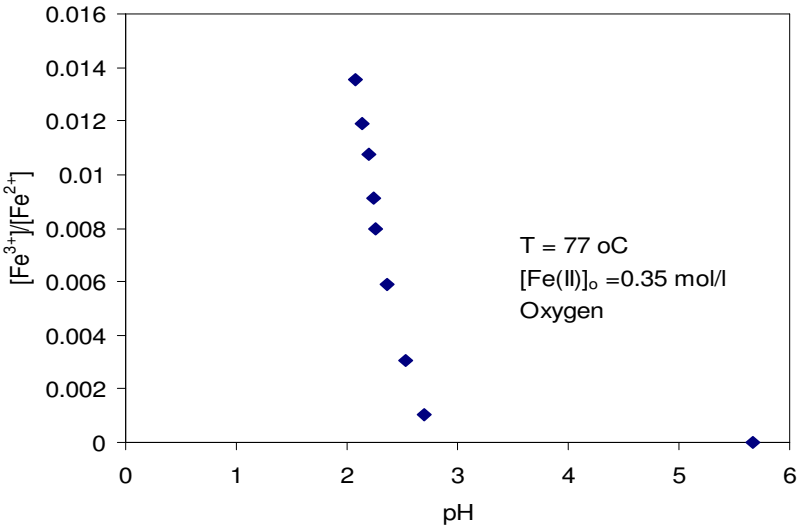

Figure 3.13 Ferric to Ferrous species in solution

3.4.6 Kinetic variables considered for modelling

For modelling purpose, systematic kinetic experiments are conducted as follows: Starting at temperature of 77 ^{o}C and using oxygen as an oxidant, runs are done for five different starting ferrous concentration. The runs are repeated for lower temperature of 55 ^{o}C and with oxygen. Finally, using air as the oxidant the same

runs are performed at 77 °C. It is not possible to repeat the runs with air at lower temperature of 55 °C) because of the slower reaction rate. From these experiments and using the method of initial rates, the oxidation rate is plotted against the initial ferrous concentrations, Figure 3.14.

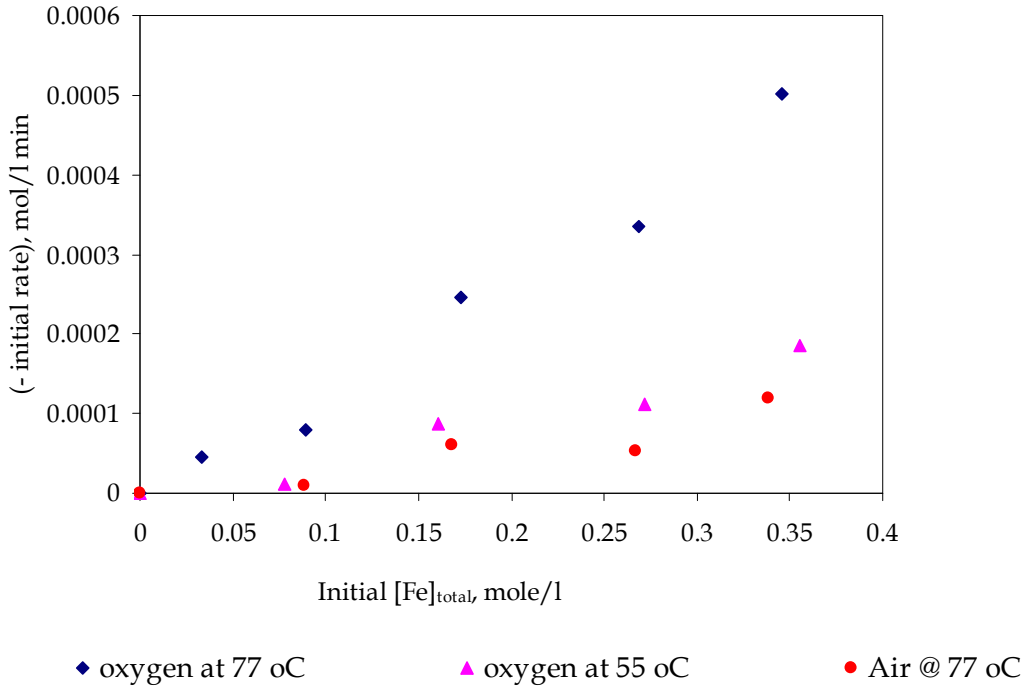

Figure 3.14 Effect of kinetic variables on the experimental rate

It is evident from the plot that the initial reaction rate depends on the starting ferrous concentration, the oxygen concentration and temperature.

4.0 MODELLING OF EXPERIMENTAL DATA

4.1 Empirical Model of Rate Equation

From section 3.3, it is evident that hardly any manganese co-precipitated with iron; therefore, approximately all the manganese remains in solution. Similarly, only a small amount of sulphate precipitates with the iron and the rest remains in solution. Since these species (manganese and sulphate) remain relatively constant in the solution and only the iron is oxidised and precipitates out, the oxidation reaction can be modelled in terms of the iron species present in the solution.

The oxidation of iron from ferrous to ferric species is given as equation 1.8 (Mathews and Robins, 1972; Chmielewski and Charewicz (1984); etc.) and presented here again for convenience as equation 4.1:

$$Fe^{2+} + \tfrac{1}{2} O_2 + 2H^+ = Fe^{3+} + H_2O \qquad \ldots \qquad (4.1)$$

If the reaction is not mass transfer controlled, an empirical rate model is initially chosen which follows the general relationship as observed by other authors (Mathews and Robins, 1972; etc.). Thus

$$r_o = k[Fe^{2+}]^{\alpha}[O_2]^{\beta}[H^+]^{\gamma}\exp(-E/RT) \qquad \ldots \qquad (4.2)$$

where α, β and γ are the reaction orders to be determined experimentally. From section 3.4.4, $[H^+]$ has negligible effect on the reaction rate (for the experimental conditions), the rate equation then reduces to

$$r_o = k[Fe^{2+}]^{\alpha}[O_2]^{\beta}\exp(-E/RT) \qquad \ldots \qquad (4.3)$$

For constant volume experimental batch reactor used, the rate of disappearance of the Fe^{2+} becomes

$$-\frac{d[Fe^{2+}]}{dt} = r_o = k[Fe^{2+}]^{\alpha}[O_2]^{\beta}\exp(-E/RT) \quad \ldots \quad (4.4)$$

Since the ferric species present in the solution is negligible (Section 3.4.5), the ferrous ion concentration can be written in terms of the total iron concentration measured by the AAS. Also, oxygen concentration is modelled in terms of saturated oxygen concentration by assuming that the reaction is not mass transfer controlled where $[O_2] \sim [O_2]_{sat}$ (Section 1.4). The rate equation then takes the form of

$$-\frac{d[Fe_T]}{dt} = K[Fe_T]^{\alpha}[O_2]_{sat}^{\beta}\exp\left(-\frac{E}{RT}\right) \quad \ldots \quad (4.5)$$

The objective is to determine what the constants; α, β, K and E are experimentally. The parameters are fitted to the initial rates using the method of least squares. The estimated values are α = 1.58, β = 0.88, E = 53.2 kJ/mol and K=1.97 x 10^8 mol/l. The reaction rate order with respect to oxygen is estimated to be 0.88. This is close to unity as found by many authors (Mathews and Robins, 1972; Chmielewski and Charewicz, 1984). The ferrous rate order on the other hand is fractional. This disagrees with some authors (Chmielewski and Charewicz, 1984, Vračar and Cerović (1997) but agrees with Rönnholm *et al* (1999). The high activation energy is in general agreement with literature (Chmielewski and Charewicz, 1984; Vračar and Cerović, 1997).

Using these estimated values from least squares, the values from rate equation (4.5) are compared to the experimental initial rates of Figure 3.14. The results are shown as Figure 4.1.

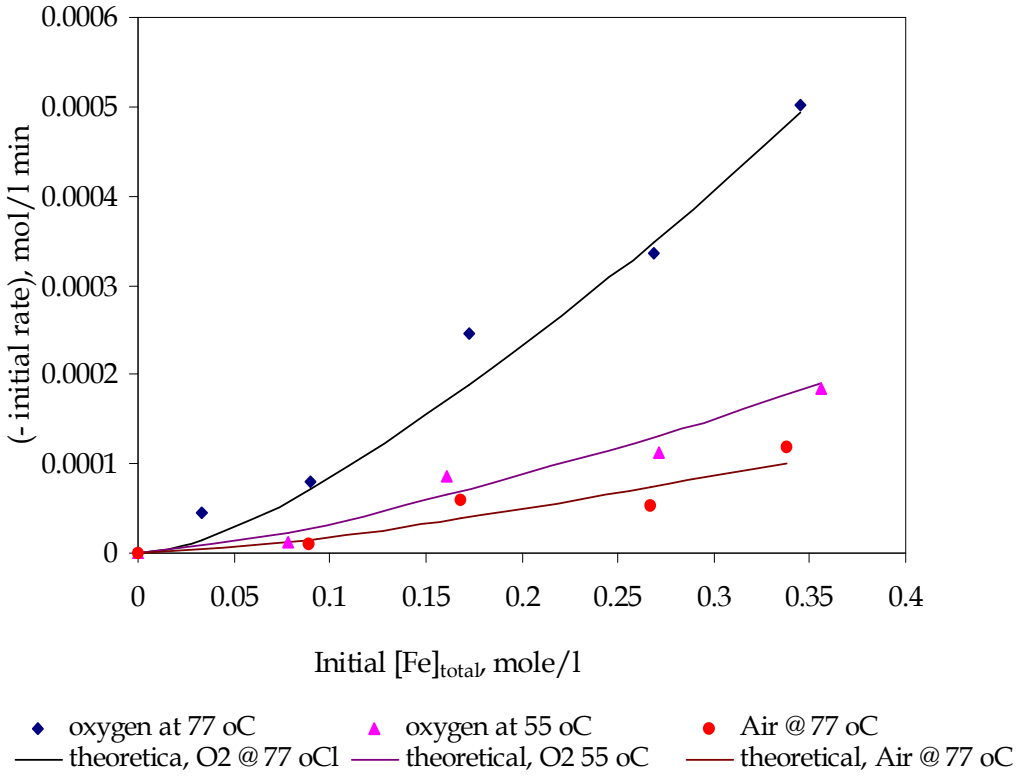

Figure 4.1 Least Squares fits to experimental initial rates

4.2 Mechanistic modelling of the reaction rate

The reaction rate model obtained thus far (Equation 4.5) is independent of hydrogen ion concentration, hence the mechanism proposed by Mathews and Robins (1972) for path 1 (Section 1.3.1) could apply. However, the derived rate law by the same authors shows a second order dependence with respect to the ferrous concentration, which is inconsistent with the fractional order obtained in section 4.1.

Rönnholm *et al* (1999) also proposed a mechanistic reaction rate expression based on non-catalytic mechanisms of the oxidation of ferrous sulphate (Section 1.3.1). The derivation of the equation by the authors is summarised in Appendix A5. The rate of oxidation of ferrous ions is given by

$$r_{Fe^{II}} = \frac{\alpha[Fe^{II}]^2\ e^{-E/(RT)}[O_2]}{1+(\alpha/\beta)[Fe^{II}]} \qquad \ldots \qquad (4.6)$$

For a constant volume batch reactor, an expression is obtained for the time dependence of the total ferrous concentration.

$$\frac{d[Fe^{II}]}{dt} = \frac{\alpha[Fe^{II}]^2\ e^{-E/(RT)}[O_2]}{1+(\alpha/\beta)[Fe^{II}]} \qquad \ldots \qquad (4.7)$$

From this model, the rate order with respect to the ferrous concentration depends on the magnitudes of the constants α and β. If α << β, the equation approximates a second order rate equation (with respect to the ferrous concentration) as proposed by many authors (Mathews and Robins, 1972; etc). Similarly, if α >>β, the equation approximates a first order rate equation. Otherwise, the rate

equation (4.7) is fractional. This is similar to the results obtained in this work. In other words, the expression describes the reaction rate modelled above as equation 4.5. Therefore, assuming that Rönnholm *et al* (1999) mechanism for the oxidation reaction is obeyed in this work, the experimental data are modelled according to this expression by estimating the parameters α, β and E in the expression.

It is necessary to reduce the number of parameters by determining the value of the activation energy. Separation of variables and integration between the limits ($t = 0$, $[Fe^{II}] = [Fe^{II}]_o$) gives after rearrangement

$$\left(\frac{1}{[Fe^{II}]}-\frac{1}{[Fe^{II}]_{,o}}\right)\frac{1}{t}=\frac{\alpha}{\beta}\ln\left(\frac{[Fe^{II}]}{[Fe^{II}]_{,o}}\right)\frac{1}{t}+\alpha[O_2]\exp\left(-\frac{E}{RT}\right) \quad \ldots \quad (4.8)$$

By plotting $\left(\frac{1}{[Fe^{II}]}-\frac{1}{[Fe^{II}]_{,o}}\right)\frac{1}{t}$ against $\ln\left(\frac{[Fe^{II}]}{[Fe^{II}{}_o}\right)\frac{1}{t}$ yields a straight line with slope α / β and an intercept of $\alpha[O_2]\exp\left(-\frac{E}{RT}\right)$. This intercept can only be obtained for $t \neq 0$. The plots for different temperatures are shown in Figure 4.2.

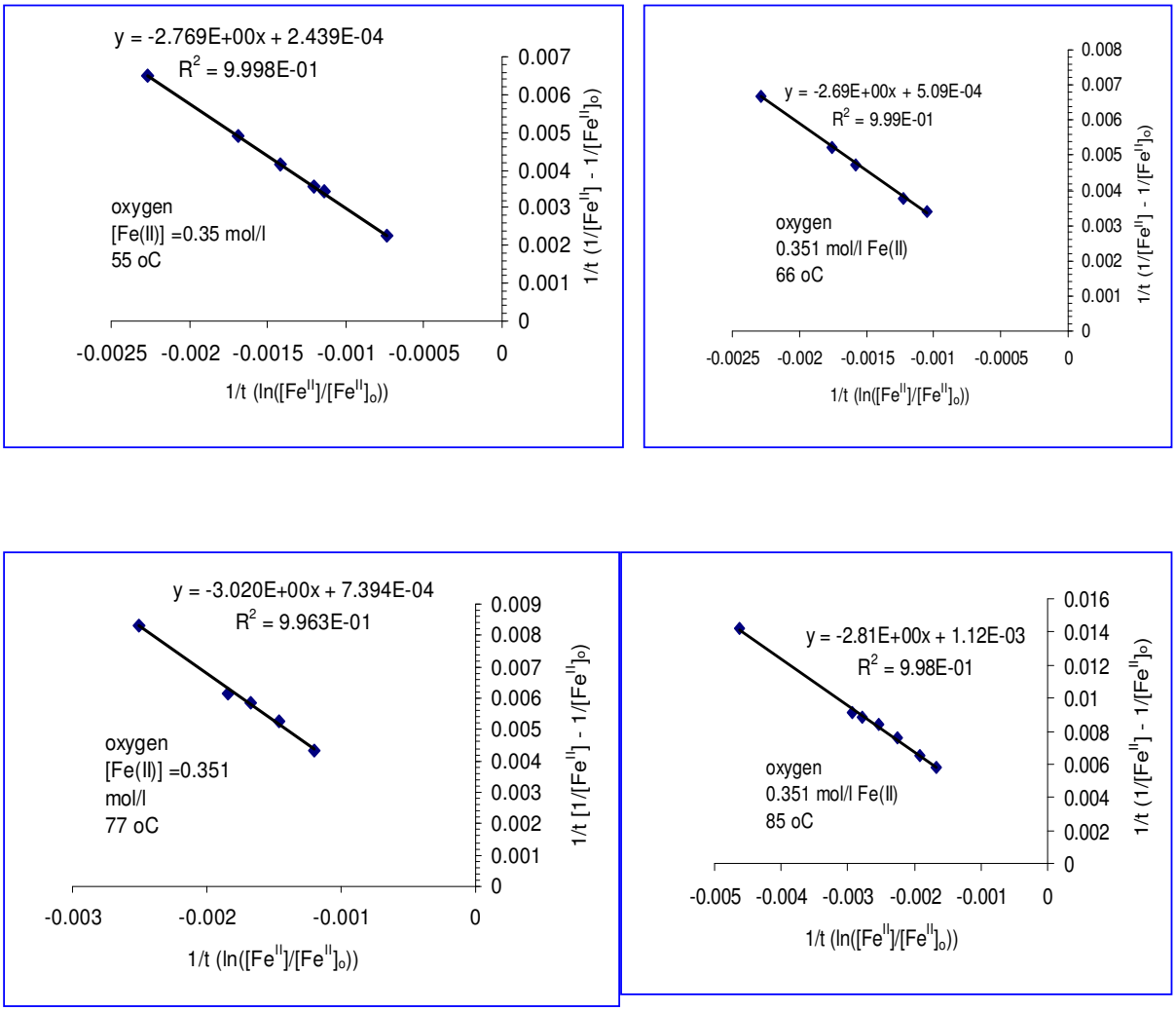

Figure 4.2 Estimation of Activation Energy from the Model presented by Rönnholm *et al* (1999)

Let the intercept be K, plotting ln*K* vs. 1/T yields a straight line with slope E/R as shown in Figure 4.3.

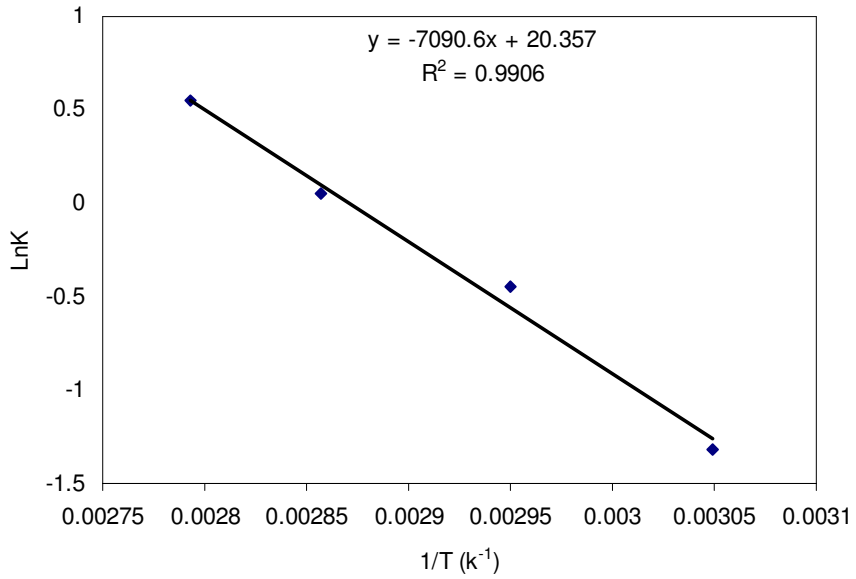

Figure 4.3 Arrhenius Plot for model by Rönnholm *et al* (1999)

The activation energy is estimated to be 59.0 kJ/mol. The high activation energy suggests that a chemical reaction is the rate controlling factor. Using this activation energy value, the parameters α and β in Equation 4.7 are then estimated by non-linear regression analysis. All the data sets collected at different temperatures, different oxidants and initial ferrous concentrations are merged together in the parameter estimation.

The following objective function is minimised in the estimation of the parameters.

$$SSE = \sum \left([Fe^{II}]_{\exp} - [Fe^{II}]_{cac} \right)^2 \quad \ldots \quad (4.9)$$

where $[Fe^{II}]_{exp}$, is the total ferrous concentration observed experimentally and $[Fe^{II}]_{cac}$, is the calculated ferrous concentrations from the model Equation 4.7.

A plot of the residual sum of squares of the errors (SSE) against the parameters α and β is shown in Figures 4.4 and 4.5 respectively.

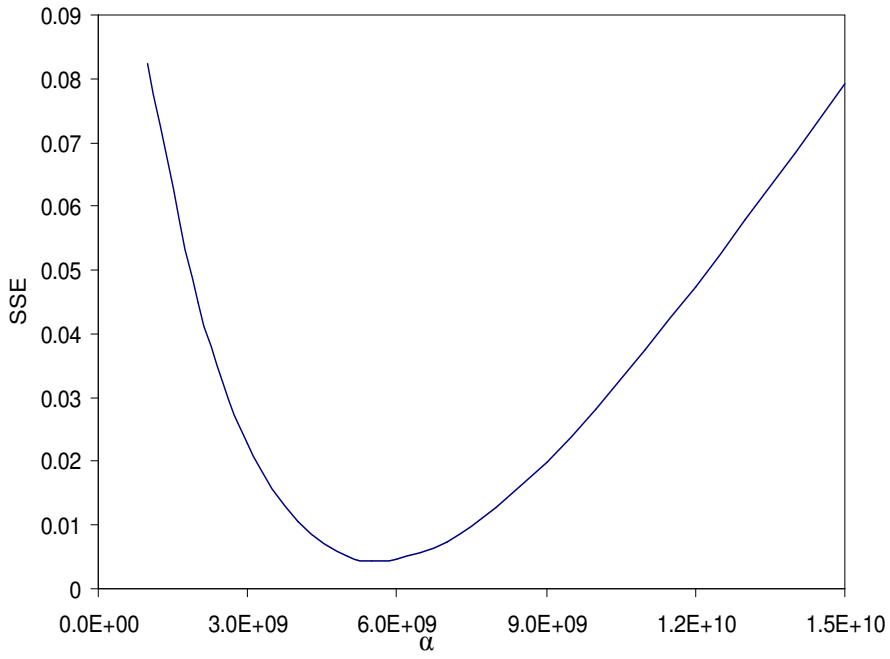

Figure 4.4 Effect of parameter α on SSE

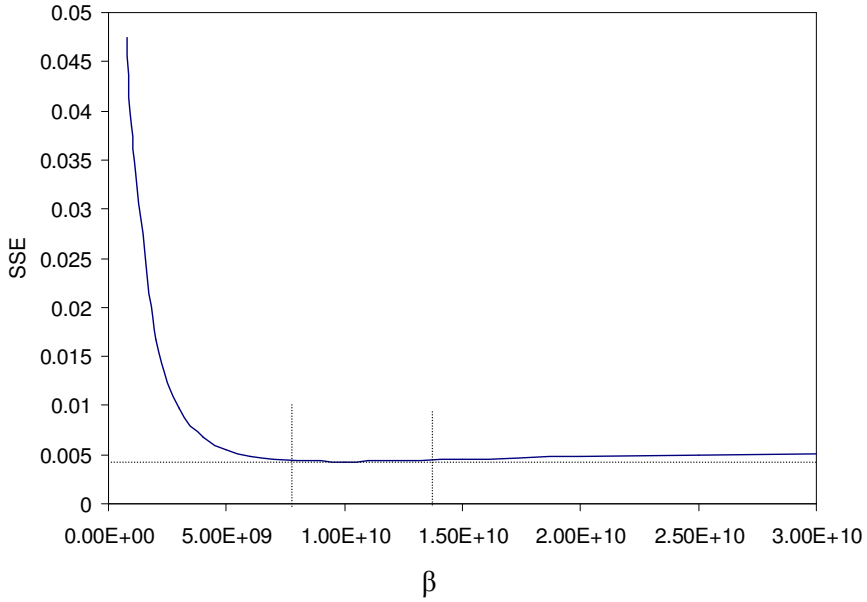

Figure 4.5 Effect of parameter β on SSE

Clearly, α is the more sensitive of the two parameters as it has the sharper minimum. β on the other hand is only sensitive below 8.0×10^9. In summary, the estimates of the parameters in Equation 4.7 are shown in Table 4.1.

Table 4.1 Estimated Parameters

Parameter	Estimated value
α	5.65×10^9 M/l. min
β	9.0×10^9 M/l. min
E	58.9 kJ/mol K

The experimental ferrous concentrations and their corresponding values predicted by the model (Equation 4.7) are graphically displayed in Figure 4.6. It can be seen that the correlation is reasonably good. Furthermore, a histogram of normal distribution of the residuals produced by the model is presented in Fig. 4.7. The normal (Gaussian) density function is superimposed on the histogram to show the extent of deviation from the normal distribution.

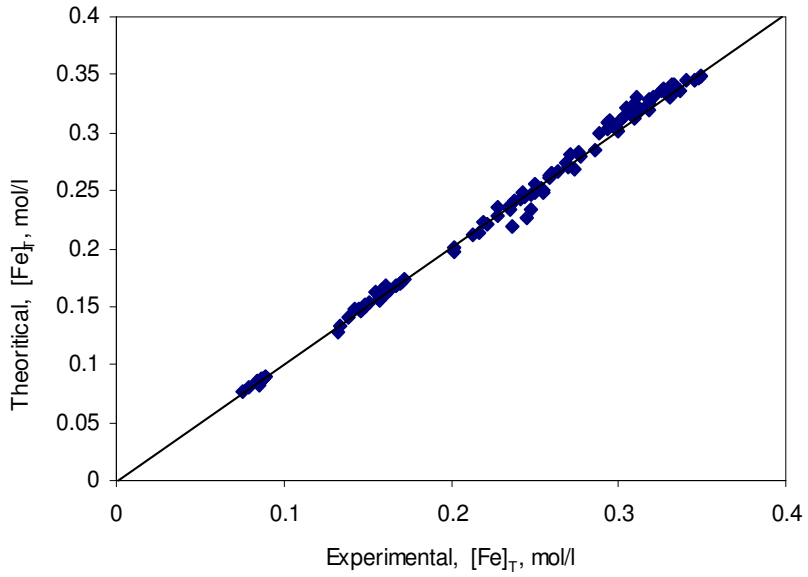

Fig. 4.6 Predicted ferrous concentration vs. experimental

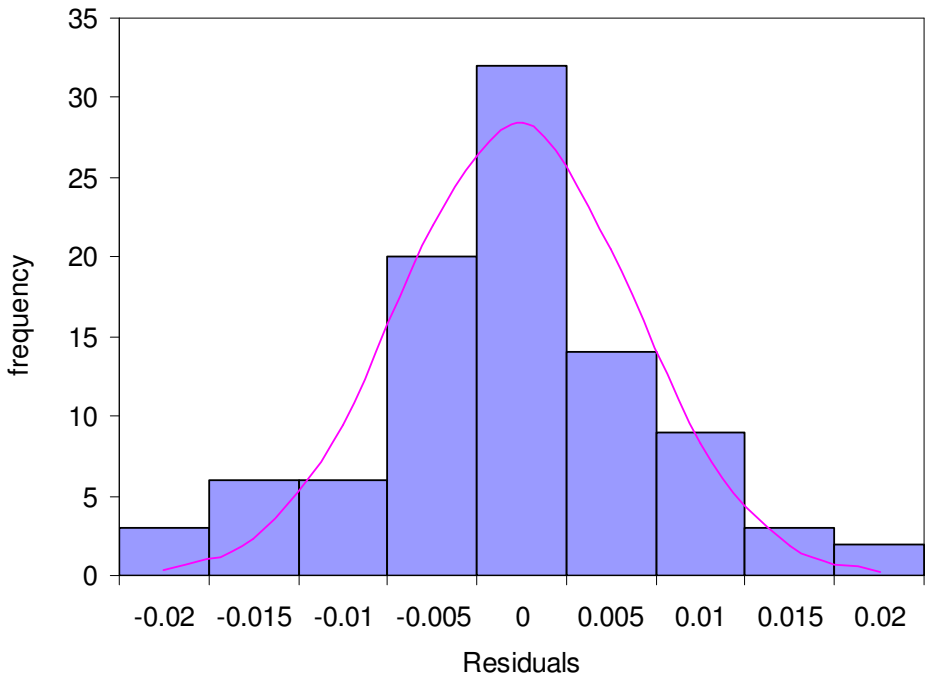

Fig. 4.7 Histogram of normal distribution of the residuals

Finally the plots of ferrous concentration as functions of time are generated according to the mechanistic model using the parameters in Table 4.1. These are shown as Figure 4.8 for oxidation using oxygen at 77 oC with different initial ferrous concentrations and compared to experimental results. Further comparisons between model prediction and experimental data can be found in Appendix A6

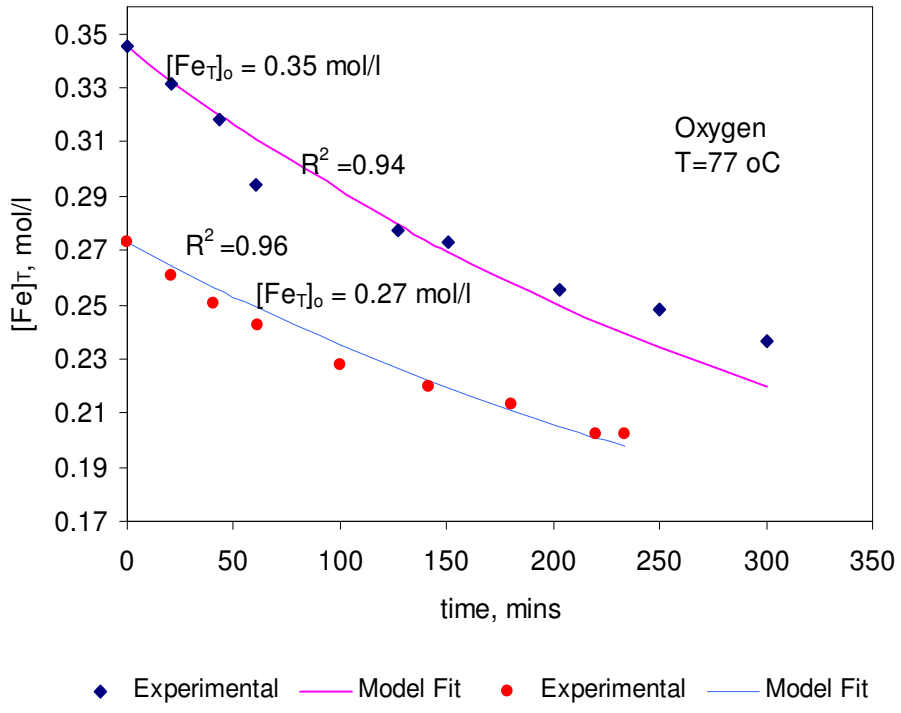

Figure 4.8 Comparison of model with experimental data

5.0 CONCLUSSIONS AND RECOMMENDATIONS

It is shown in this work that iron can be selectively separated from manganese sulphate solutions at the selected experimental conditions (5 – 20 g/l Fe (II)). The analysis of the solids proves that iron is precipitated out as an easily filterable goethite ($Fe_2O_3.H_2O$) compound. Although this compound seems to be the dominant species in the solids, small amounts of sulphate and manganese contaminants are also evident. Running the experiment for longer periods and lower ferrous concentrations (2 g/l) made no difference to the composition or form of solid precipitate formed.

The magnitude of the activation energy of reaction obtained indicates that the reaction rate is controlled by a chemical reaction step. The effect of the main variables are identified leading to an adequate correlation of the experimental rate data with the following empirical model:

$$-r_{Fe} = 1.97\times10^{8}\,[Fe]_T^{\,1.58}\,[O_2]_{sat}\exp\left(-\frac{53.2\ KJ/mol}{RT}\right),\ \text{(Mol/l. min)}$$

This shows a fractional order with respect to the ferrous concentration. This is in agreement with the model proposed by Rönnholm *et al* (1999) based on non-catalytic mechanism of the oxidation of ferrous sulphate. The experimental rate data is also fitted to a mechanistic model proposed by Rönnholm *et al* (1999), and the following rate expression is obtained

$$-r_{Fe^{II}} = \frac{5.65\times10^{9}\,[Fe^{II}]^2\ e^{-58900/(RT)}\,[O_2]_{sat}}{1+(5.65\times10^{9}/9.0\times10^{9})[Fe^{II}]} \qquad \text{(Mol/l. min)}$$

It is recommended that future experimental work in this field should attempt to maintain a higher pH throughout the run. This could be done by periodically adding small amounts of MnO to the reaction vessel at predetermined times. In this way, soluble iron levels would be reduced to very low values, which would be close to plant practice.

From modelling point of view, the higher pH over an extended period should be able to clarify some of the literature postulates, e.g. under neutral conditions the reaction rate becomes first order with respect to the ferrous ions (Zhang *et al*, 2000).

NOMENCLATURE

α, β	*kinetic constants determined experimentally (as proposed by Rönnholm et al (1999))*
a_o	*Interfacial area of all bubbles per unit volume of aqueous phase*
a_{oxd}	*Activity of oxidised species*
a_{red}	*Activity of reduced species*
C_i	*molar concentration of species I, mol/l*
C_{Fe}, $[Fe_T]$	*Total Iron concentration in solution, mol/l*
C_{O_2}, $[O_2]$	*Molecular Oxygen concentration, mol/l*
$C_{Fe,\ exp}$	*Total Iron concentration observed experimentally, mol/l*
$C_{Fe,\ calc}$	*Total Iron concentration calculated, mol/l*
D_{O_2}	*Molecular Diffusivity of Oxygen*
E	*Activation Energy, kJ/mol*
E_h	*Solution potential, V*
E_o	*Standard solution potential, V*
F	*Faraday Constant, J.mol-1.V-1*
$[Fe(II)]$,$[Fe^{II}]$	*Total ferrous concentration, mol/l*
$[Fe(III)]$, $[Fe^{III}]$	*Total ferric concentration, mol/l*
$[Fe^{2+}]$	*Ferrous ion concentration, mol/l*
$[Fe^{3+}]$	*Ferric ion concentration, mol/l*
ΔG^o	*Standard Gibbs Free Energy,J/mol*
$[H^+]$	*hydrogen ion concentration, mol/l*
$[HSO_4^-]$	*bisulphate ion present in solution, mol/l*
K_p,K	*Equilibrium Constant*
K_m	*Mass Transfer Coefficient*
k	*rate constant*

k''	*lumped rate constant*
K''	*lumped equilibrium constant*
N_i	*moles of species i, mol*
n	*electrons lost or gain in a redox reaction*
p_{O_2}	*Partial pressure of Oxygen, atm*
$[O_2]_{sat}$	*Saturated Oxygen Concentration, mol/l*
r_i	*rate of formation of species i, mol/l min*
R	*Gas Constant, J/mol K*
$[SO_4^{2-}]$	*Sulphate ion concentration, mol/l*
T	*Temperature, ^oC*
V	*Total reactor volume, l*
*	*Surface site (interfacial quantity if used as superscript)*
+/-	*superscripts indicate cation / anion*
δ	*Apparent film thickness*

REFERENCES

1. Akdogan, G. and Eric, H. (1995). Kinetics of the Solid-State Carbothermic Reduction of Wessel Manganese Ores. *Metallurgical and Materials Transactions B*, **26B**, 13-24.
2. Arslan, C. and Arslan, F. (2003). Thermochemical review of Jarosite and Goethite Stability Regions at 25 ^{o}C and 95 ^{o}C, *Turkish J. Eng. Env. Sci*, 27: 45 – 52.
3. Barin, I. (1989). *Thermochemical Data of Pure substances, Parts 1 and 2*, VCH,
4. Barin, I., Knacke, O. and Kubaschewski, O. (1977). *Thermochemical properties of inorganic substances (supplement)*. Springer-Verlag, Berlin.
5. Burkin, A. R. (2001). *Chemical Hydrometallurgy* (*theory and Principles*), Imperial College Press.
6. Chmielewski, T. and Charewicz, W. A. (1984). The oxidation of Fe (II) in aqueous sulphuric acid under oxygen pressure. *Hydrometallurgy*, **12**, 21 – 30
7. Crundwell, F. K. (1985). Kinetics of the leaching of spharlerite in acidic ferric sulphate in the presence and absence of oxygen, MSc. Thesis.
8. Das, S. C., Sahoo, P. K. and Rao, P. K. (1982). Extraction of manganese from low-grade ores by $FeSO_4$ leaching, *Hydrometallurgy*, **8**, pp 35 – 47.
9. Davey, P. T. and Scott, T.R (1975). Formation of β-FeOOH and α-Fe2O3 in the goethite process. *Transactions of the Institution of Mining and Metallurgy*, Section C, **84**, 83-86.
10. Davey, P. T. and Scott, T.R (1976). Removal of iron from leach liquors by the "goethite" process, *Hydrometallurgy*, **2**, 25 – 33.
11. Dutrizac, J.E. and Monhemius, A.J. (1986). *Iron control in hydrometallurgy*. Elles Horwood limited, England.

12. Elvers, B., Hawkins, S. and Schulz, G. (1990). *Ullmann's Encyclopedia of Industrial Chemistry*. 5th edn, **A 16.**
13. Ferron, C. J., Kwateng, D. O. and Duby, P.F. (1991). Kinetics of the precipitation of goethite from ferrous sulphate solution using oxygen-sulphur dioxide mixtures, *The Minerals, Metals and Matarials Society - EPD Congress*. 165 – 173
14. Godsell, A.J. and Fray, D.J. (1990). Metallic Solvent Extraction of Manganese and Titanium fom Ferroalloys. *Metallugical Transactions B*, **21B**, 217 – 228
15. George, P. (1954). The oxidation of ferrous perchlorate by molecular oxygen. *J. Chem. Scoc.* **4**, 4349-4359
16. Harris, M., Meyer, D.M and Auerswald, K. (1977). The production of electrolytic manganese in South Africa. *Journal of the South African Institute of Mining and Metallurgy*, **77** (7), 137-142
17. Hayes, P. C. (1993). *Process Principles in Minerals and Materials Production*, Hayes Publishing Co., Queensland, Australia
18. Huffman, R. E. and Davidson N. (1956). Kinetics of the ferrous Iron-Oxygen Reaction in Sulfuric Acid Solution, *J. Am. Chem. Soc.*, **53**: 4837 – 4842.
19. Iwai, M., Majima, H. and Awakura, Y. (1982). Oxidation of Fe (II) in sulphuric Acid Solutions with Dissolved Molecular Oxygen. *Metallurgical Transactions*, **13B**, 311-318.
20. Limpo, J. L. and de la Cuadra, A. (1977). Study of F^{3+} - SO_4H_2 – $SO4^{2-}$ (Its application in hydrometallurgy), *Rev. Meatll*, **13**, No. 2: 67-79
21. Lajunen, L.H. J (1992). *Spectrochemical Analysis by Atomic Absorption and Emission*, The Royal Society of chemistry

22. Mathews, C.T., and Robins, R.G. (June 1972). The oxidation of aqueous ferrous sulphate solutions by molecular oxygen, *Proceedings of Australian Institute of Mining and Metallurgy*, No. 242: 47-56
23. McAndrew, R.T., Wang, S. S. and Brown, W. R. (January 1975). Precipitation of iron compounds from sulphuric acid leach solution, *Canadian Institution of Metallurgy Bulletin*, **68**, No. 753: 101-110.
24. Narita, E., Lawson, F. and Han, K. N. (1983). Solubility of oxygen in aqueous electrolyte solutions, *Hydrometallurgy*, **10**, 21 –27.
25. Rönnholm, M. R., Wärnå, J., Salmi, T., Turunen, I. and Luoma, M. (1999). Kinetics of oxidation of ferrous sulfate with molecular oxygen, *Chemical Engineering Science*, **54**, 4223 – 4232.
26. Rönnholm, M. R., Wärnå, J., Salmi, T., Valtakari, D. and Laine, E. (2001). Kinetics and mass transfer effects in the oxidation of ferrous sulfate over doped active carbon catalysts, *Catalysis Today*, 66, 447 – 452.
27. Rönnholm, M. R., Wärnå, J. and Salmi, T. (2002). Two – and three phase oxidation of ferrous sulfate to ferric sulfate from intrinsic kinetics to diffusion-affected industrial kinetics, *Chemical Engineering and Processing*, **41**, 753 - 760
28. Sahoo, P.K. et al (1979). Separation of Iron, *J. Chem.Tech.Biotechnology*, **29**, 307 – 310.
29. Sully, A.H. (1955) *Manganese*, Butterworths Scientific Publications, London.
30. Sykes, A.G. (1966) *Kinetics of Inorganic reactions*, Pergamon Press, Oxford
31. Van Loon, J. C. (1980). *Analytical Absorption Spectroscopy*, Academic Press, Ney York.

32. Vračar, R. Ž. and Cerović, K. P. (1997). Kinetics of oxidation of Fe (II) ions by gaseous oxygen at high temperatures in an autoclave, *Hydrometallurgy*, **44**, 113-124.
33. Welz, B. (1985). *Atomic Absorption Spectroscopy*, 2nd completely revised edition, VCH.
34. Zhang, W. David, M. and Singh, P. (2000). Iron oxidation by SO_2 / O_2 in acidic media, Part II. Effect of copper, *Hydrometallurgy*, **58**, 117 – 125.
35. De Bruijn, T.J.W. et. Al., (1980). *Modelling of the reduction of manganese oxides with hydrogen*., Chem. Engng. Sci., 1591-1600.
36. Van Arsdale, G. (1965). *Hydrometallurgy of Base Metals*, McGraw-Hill, New York

APPENDICES

Appendix A1: Atomic Absorption Spectrometry (AAS)

The iron and manganese contents from each run are significantly high (32 000 ppm for Mn and 5 000 – 20 000 ppm for iron) that large dilution is required in order to analyse them on the AAS.

Principles of AAS

Atomic Spectroscopy technique includes atomic absorption, atomic emission and atomic fluorescence spectroscopy (Van Loon, 1980). Each involves valence electron transitions yielding radiation with wavelengths in the ultraviolet region of the spectrum. In atomic spectra, electron orbiting in an atom is characterized by the quantum numbers n and l. When the electron undergoes a transition from a higher energy level (Enl) to a lower energy level (E n_1l_1), light frequency is given off as:

$$v = (E_{nl} - E\,n_1 l_1)/h = \Delta E/h \qquad \ldots \qquad (A1.1)$$

In terms of wavelength,

$$\lambda = c/v = hc/\Delta E$$

Where h and c are Planck's constants and velocity of lights respectively. Thus, electronic transitions can be discussed in terms of frequency v, energy E, and wavelength λ. The most frequently used is the wavelength. An element can undergo many electronic transitions, resulting in series of sharp lines known as spectrum, which is uniquely characteristic of each element.

Emission and absorption can be related as shown in Figure. A1.1

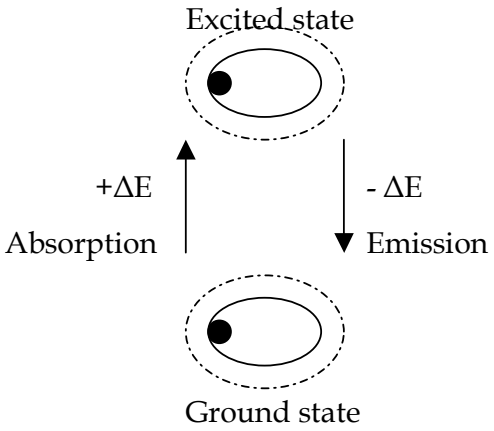

Figure A1.1 Emission and absorption of energy by a valence electron

Absorption occurs when an electron of an atom in the ground state absorbs a quantum of energy (+ΔE) and undergoes a transition to the excited state. Similarly, emission occurs when this quantum of energy is released and the electron is returned to the ground state. This transition of to and from the ground state is known as *resonance transition*- most useful analytical lines used in atomic absorption spectroscopy. Which transitions are permitted or forbidden are govern by spectroscopic rules based on quantum mechanics.

Relationship between Absorption and Concentration

The two laws governing the absorption of monochromatic radiation are:

Lambert's law: light absorbed in a transparent absorption cell is independent of incident light intensity. Each successive layer of absorbing medium absorbs an equal fraction of the light.

Beer's law: Absorption of light is exponentially proportional to the number of absorbing species in the path of the light beam. Based on these two laws, if incident beam of monochromatic radiation I_O falls on absorption cell of length b and the transmittance is given by

$$T = e^{-kbc} \quad \ldots \quad \text{(A1.2)}$$

Since

$$\log_{10}(1/T) = \log_{10}(I_O / I) = abc \quad \ldots \quad \text{(A1.3)}$$

and

$$\log_{10}(I_O / I) = A \quad \ldots \quad \text{(A1.4)}$$

where A is the absorbance, A = abc, a is constant for a given system and c concentration of the analyte in the flame. This expression known as Beer-Lambert law, predicts a linear relationship between absorbance and concentration as long as a and b remains constant. The linear relationship is between the concentration of the analyte atoms in the atomizer and not necessary the analyte in the solution. To obtain the latter it is therefore necessary to avoid interference (see later).

Atomic absorption spectrometer (AAS) measures the absorption of optical radiation by atoms in the gaseous state. The technique is relative and not absolute, in other words quantitative results can only be obtained by comparison with reference solutions or reference materials. This means reference measurements must always be made. Through choice of suitable calibration technique, many interferences can be eliminated. According to Welz (1985),

different calibration techniques are available and demands are made with respect to accuracy, precision and speed. Few of these techniques are highlighted below:

Analytical Curve Technique

As Welz (1985) explains, this is the simplest and quickest of the technique that uses direct comparison of the sample solution with reference solutions. The calibration function is established by plotting measurements (absorbance) for set of calibrations solutions against their concentrations. The zero member has an absorbance of zero while the highest member has an absorbance equivalent to the highest expected concentration of the sample solution (see Figure A1.2 below). A linear calibration function means, BEER-LAMBERT law is obeyed and the curve passes through the origin. Concentrations of the element to be analysed in the sample solution is then estimated from the relationship:

$$c_{analyte} = \frac{A_{analyte}}{A_{reference}} \cdot c_{reference} \qquad \ldots \qquad (A1.5)$$

Where

$c_{analyte}$ = Concentration of the element to be analysed

$c_{reference}$ = Concentration of the reference solution

$A_{reference}$ = Absorbance of the reference solution

$A_{analyte}$ = Absorbance of the element to be analysed

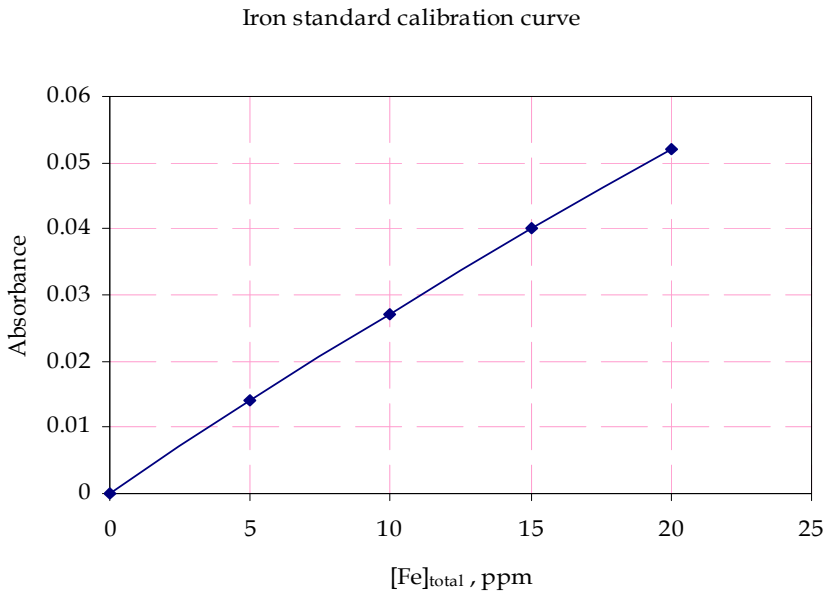

Figure A1.2 Analytical curve technique

It is also common to obtain calibration graphs with departures from ideality. I.e. it is common for the graphs to bend towards the concentration axis. As Van Loon (1980) explains, two common causes are postulated by many researches of this behaviour. Both causes result from failure of the monochromator and the slit system to prevent multiple, closed spaced lines from reaching the detector. If the graph curves more towards the concentration axis, this could be the cause of line broadening. Line Broadening occurs due to self–absorption. The greatest cause of this broadening, in a good hollow-cathode lamp, is the use of excessive lamp currents. To maximise the chance of obtaining good linear calibration curves, Van Loon (1985) suggested that the following procedures should be followed:

The manufacturers recommended current should be used. Higher values can result in serious line broadening. Narrow slit width consistent with acceptable signal to noise ratio should be used; in most cases manufacturers recommendation should be followed.

Apart from the above technique, bracketing and analyte addition techniques can also be used for calibration. For more on these techniques, the reader is referred to Welz (1985).

Interferences

As mentioned above, absorption spectrometric method is relative. The signal produced by the sample solution is compared to the signals caused by the reference solutions. If the samples and the references are behaving differently during the measurements, interferences will be seen. Interference in flame AA techniques include the following:

Chemical interference occurs when the analyte is contained in a chemical compound that is not broken down by the flame. With *Ionisation interference*, the analyte is partly ionised in the hot flame leading to decreased absorption signals. This interference is important for elements with low ionisation potentials (e.g. alkaline metals). *Physical interference* originates from changing physical characteristics of the solutions to be analysed (viscosity, temperature, etc). Finally, *atomic spectral interference* occurs when absorption profile of another element overlaps that of the analyte within the spectral line width of the emission line of source.

Analytical Analysis of Samples

The make of the AAS used is that of Varian Flame Atomic Absorption Spectrometry. The instrument allows for the option of using atomic absorption or flame emission for analysing the analyte. Lajunen (1992) suggested, for iron and manganese, atomic absorption be used. The recommended settings by the manufacturer for the identifications of these elements are tabulated below.

Table A1.1 Manufacturers recommendation for AAS settings

Fixed parameters		
Lamp Current	5 mA	
Fuel	Acetylene	
Support	Air	
Flame stoichiometry	Oxidising	
Variable parameters		
Iron, Fe		
Wavelength, nm	Slit width, nm	Optimum working range, µg/ml
248.3	0.2	0.06 – 15
372.0	0.2	1 – 100
386.0	0.2	1.5 – 200
Manganese, Mn		
279.5	0.2	0.02 – 5
403.1	0.2	0.5 – 60

As Welz (1985) discusses, 'better' readings are obtained by using the first two wavelengths (lower concentrations of the standards). As a result, the concentrations of the elements to be analysed is diluted 1000 times (for the iron) and 10 000 times (for the manganese) to get to the required concentrations. Five standard samples, 1, 5 10, 15 and 20 ppm are prepared for the iron; and three standard samples, 1, 3, and 5 ppm for the manganese. These standards are prepared from 1000 ppm standards sold commercially. Preliminary measurements showed lower readings for the iron concentrations. Since manganese and iron are closely located on the periodic table, the lower readings of the concentrations are assumed to be as a result of the interferences caused by the two elements. To eliminate this, the standards are prepared from the starting solutions for the runs. For an example, 5 ppm standard is prepared from solution containing starting iron concentration of 5 g/l and 32 g/l manganese. 1 ml of this is then diluted in 1000 ml distilled water. A drop of sulphuric acid is added to prevent any oxidation of the iron. The standards are kept for all the entire runs. Reproducible measurements were then obtained after this.

The spectroscopy used is digitalised one and permits the entry of the concentration of the elements in the sample solution. The spectrometer then determines the calibration function automatically and presents the analytical results in the desired units (in this case ppm).

Figure A1.2 is typical iron standard calibration curve used for the iron analysis. Concentrations of set of calibration solutions are plotted against their absorbance. The concentration of the sample is determined from its absorbance measure by interpolation.

Appendix A2: Construction of Pourbaix Diagrams

The following equilibrium reactions are considered for constructing the diagram of Fe – H_2O system.

Equilibrium between solids

$Fe\ (s) + H_2O = FeO\ (s) + 2H^+\ (aq) + 2e$ … (A2.1)

$3Fe\ (s) + 4H_2O = Fe_3O_4\ (s) + 8H^+\ (aq) + 8e$ … (A2.2)

$3FeO\ (s) + H_2O = Fe_3O_4\ (s) + 2H^+\ (aq) + 2e$ … (A2.3)

$2Fe_3O_4\ (s) + H_2O = 3Fe_2O_3\ (s) + 2H^+\ (aq) + 2e$ … (A2.4)

$2FeO\ (s) + H_2O = Fe_2O_3\ (s) + 2H^+\ (aq) + 2e$ … (A2.5)

Equilibrium between solids and ions

$Fe\ (s) = Fe^{2+}\ (aq) + 2e$ … (A2.6)

$Fe^{2+}(aq) + H_2O = FeO\ (s) + 2H^+\ (aq)$ … (A2.7)

$3Fe^{2+}\ (aq) + 4H_2O = Fe_3O_4\ (s) + 8H^+(aq) + 2e$ … (A2.8)

$2Fe^{2+}\ (aq) + 3H_2O = Fe_2O_3\ (s) + 6H^+\ (aq) + 2e$ … (A2.9)

$Fe^{3+}(aq) + 2H_2O = FeOOH\ (s) + 3H^+\ (aq)$ … (A2.10)

Equilibrium between ions

$Fe^{2+}\ (aq) = Fe^{3+}\ (aq) + e$ … (A2.11)

$Fe^{3+}\ (aq) + 4H_2O = FeO_4^{2-}\ (aq) + 8H^+\ (aq) + 3e$ … (A2.12)

Stability limits of water

$O_2 + 4H^+ + 4e = 2H_2O$ … (A2.13)

$2H^+ + 2e = H_2$ … (A2.14)

The calculations involve lots of repetitions; therefore only sample calculation is shown here.

It is obvious that the equilibrium reaction (A2.1) involves electrons; therefore the Nernst equation is applied:

$$E = E^o - \frac{RT}{zF}\ln\frac{\{\text{Re}\,duced\ state\}}{\{Oxidised\ state\}}$$

Where R and F are the gas constant = 1.978 cal.mol^{-1}.K^{-1}and Faraday constant = 23.06 kcal.mol-1.V-1 respectively. The standard potential, E^o is calculated from the standard free Gibbs energy according to the relationship:

$$-\Delta G = z\,E^o\,F = RT\ln K$$

Where K is the equilibrium constant for the reaction. Again the reaction shows a pH dependence to form the oxide and two electrons are involved z = 2. The standard free energy change of this reaction at 298 K is thus:

Fe-FeO

$$\Delta G^o = \Delta G^o{}_{FeO} + 2\Delta G^o{}_{H^+} - \Delta G^o{}_{Fe} - \Delta G^o{}_{H_2O}$$
$$= -1.908\frac{kcal}{mol}$$

So that the standard potential is obtained from

$$E^o = -\frac{\Delta G}{zF} = -0.0414V$$

For non standard conditions of the reaction, the Nernst equation is expressed in terms of activities of the species involved in the reaction as:

$$E = E^o - \frac{RT}{zF}\ln\frac{[FeO][H^+]^2}{[Fe][H_2O]}$$

Assuming unit activities for pure species of solids and water, the equation simplifies to

$$E = E^o - 0.0059\ pH \quad = -0.0414 - 0.0059\ pH$$

Assuming unit activities for pure species of solids and water, the equation simplifies to

$$E = E^o - 0.0059\ pH = -0.0414 - 0.0059\ pH \quad \ldots \quad (A2.14)$$

Which shows the change of potential as pH changes. This calculation was repeated for all the reactions deemed necessary for the construction of the diagram. The O_2 and H_2 lines were drawn by assuming unit fugacities of oxygen and hydrogen respectively.

Similar calculation is repeated for all other reactions.

Predominance Area Diagram for Mn – H_2O system at 298.15 K

As discussed above, similar E – pH diagram is drawn for Mn – H_2O system. The following reactions (Pourbaix, 1986) are considered

Equilibrium between solids

$Mn\ (s) + H_2O = MnO\ (s) + 2H^+\ (aq) + 2e$ … (A2.15)

$E = -0.727 - 0.0591\ pH$

$3MnO\ (s) + H_2O = Mn_3O_4\ (s) + 2H^+\ (aq) + 2e$ … (A2.16)

$E = 0.462 - 0.0591\ pH$

$2Mn_3O_4\ (s) + H_2O = 3Mn_2O_3\ (s) + 2H^+\ (aq) + 2e$ … (A2.17)

$E = 0.689 - 0.0591\ pH$

$Mn_2O_3\ (s) + H_2O = 2MnO_2\ (s) + 2H^+\ (aq) + 2e$ … (A2.18)

$E = 1.014 - 0.0591\ pH$

Equilibrium between solids and ions

$Mn\ (s) = Mn^{2+}\ (aq) + 2e$ … (A2.19)

$E = -1.179 - 0.0295 \log (Mn^{2+})$

$Mn^{2+}(aq) + H_2O = MnO\ (s) + 2H^+\ (aq)$ … (A2.20)

$\text{Log}(Mn^{2+}) = 15.31 - 2pH$

$3Mn^{2+}\ (aq) + 4H_2O = Mn_3O_4\ (s) + 8H^+(aq) + 2e$ … (A2.21)

$E = 1.824 - 0.2364pH - 0.0886 \log(Mn^{2+})$

$2Mn^{2+}\ (aq) + 3H_2O = Mn_2O_3\ (s) + 6H^+\ (aq) + 2e$ … (A2.22)

$E = 1.443 - 0.173pH - 0.0591 \log (Mn^{2+})$

$Mn^{2+}(aq) + 2H_2O = MnO_2\ (s) + 4H^+ + 2e\ (aq)$ … (A2.23)

$E = 1.228 - 0.11182pH - 0.0295 \log (Mn^{2+})$

$MnO_2\ (s) + 2H_2O = MnO_4^-\ (aq) + 4H^+ + 2e$ … (A2.24)

$E = 1.692 - 0.0788pH - 0.0197 \log (MnO_4^-)$

Appendix A3: Rate Curves

The following are more of the experimental rate curves obtained for different oxidant and different initial ferrous concentration.

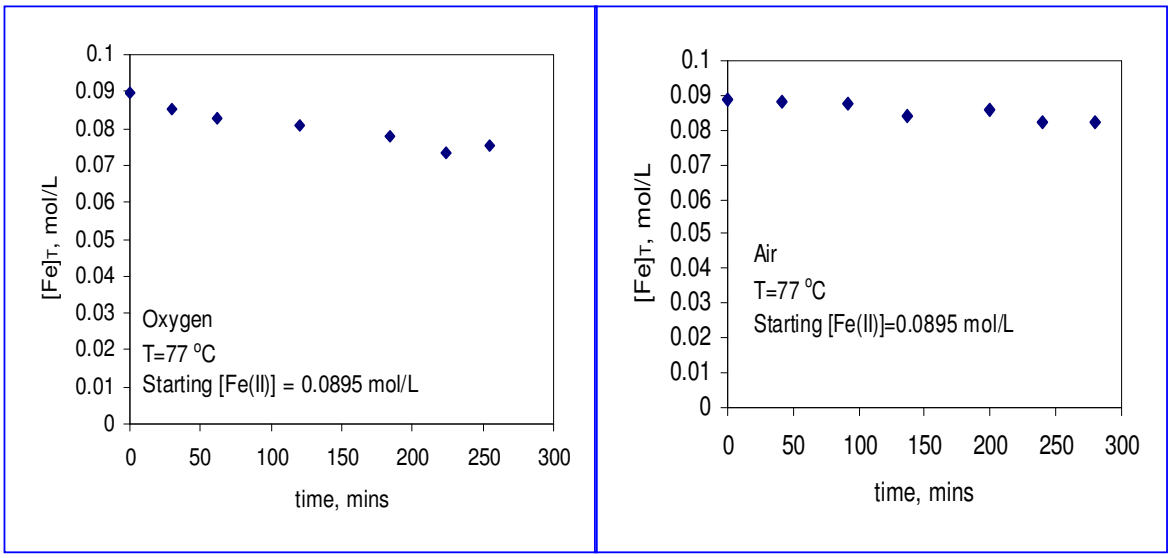

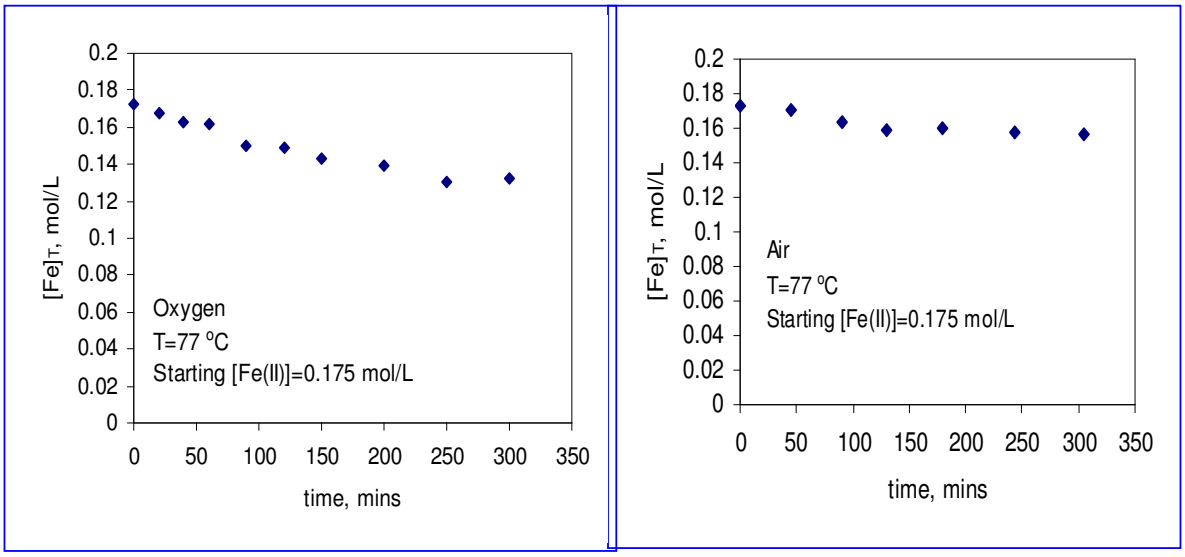

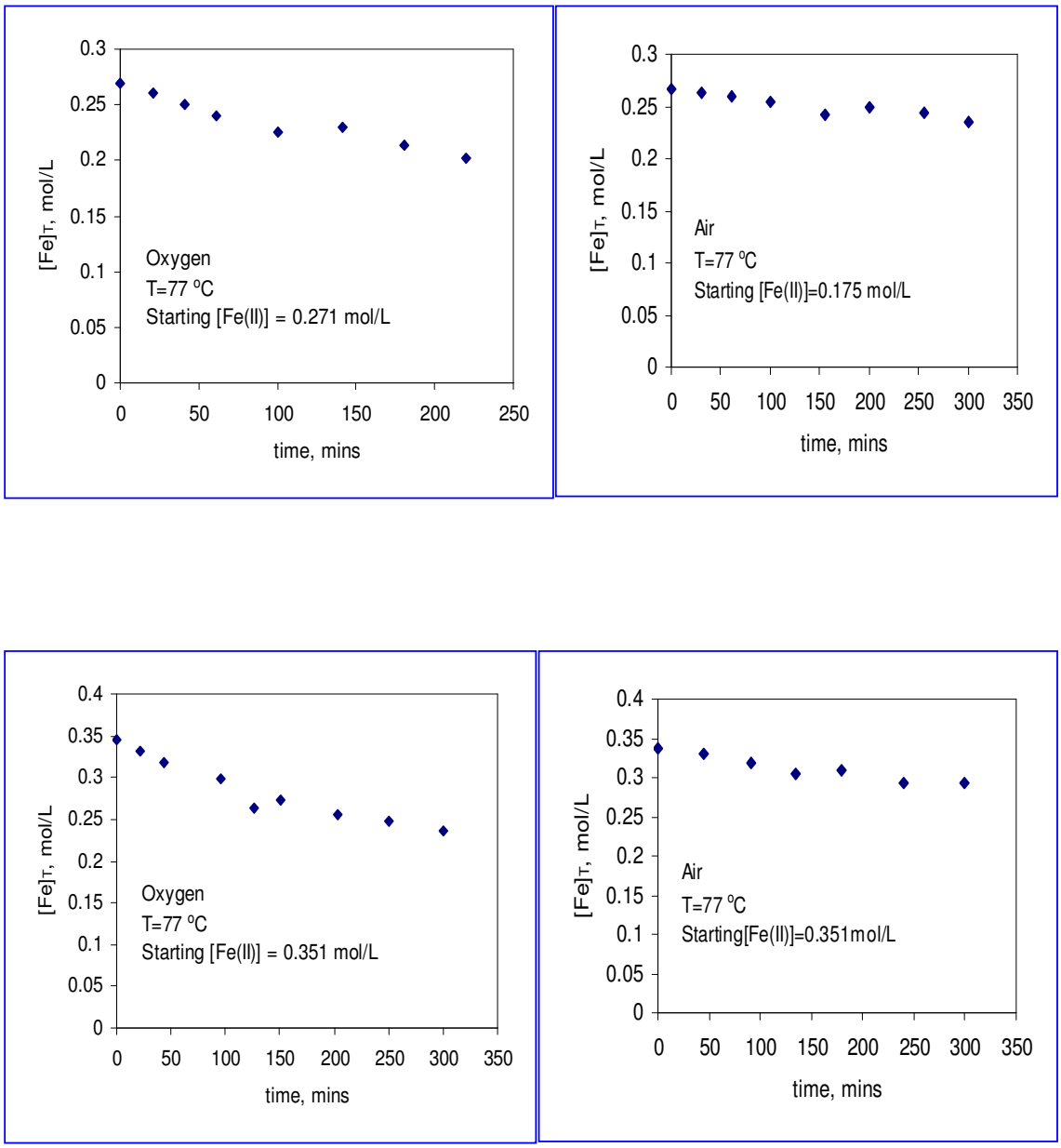

Fig.A3.1 *Experimental rate curves*

Appendix A4: Gravimetric Analysis of Sulphates as Barium Sulphate

The analysis of the sulphates involves the weighing of the sample material (to be analysed), dissolving in water, adding $BaCl_2$ solution. Barium sulphate is slightly soluble in water; therefore this compound immediately precipitates from the solution (white precipitate). The reaction may be represented by the net equation:

$$Ba^{2+}(aq) + SO_4^{2-}(aq) = BaSO_4(s) \quad \ldots \quad (A4.1)$$

Experimental Procedure

Reagents Used: Unknown Sulphate Solid Sample
0.5 M $BaCl_2$ Solution
0.1 M AgNO3 Solution
32 % HCl Solution

1) Approximately 0.4000 g of unknown sulphate solid sample is weighed into 250-ml beaker.
2) The solid sample is dissolved in approximately (10 –15) -ml HCl solution (to get all the solids dissolved). Once dissolved, about 150 ml of distilled water is **slowly** added to the acidic solution and heated to the boiling point (without actually boiling the sample). Drops of $BaCl_2$ solution are added from medical dropper until precipitation appeared to be completed.
3) The precipitate is allowed to settle and then few drops of $BaCl_2$ are added (without disturbing the precipitate) to test for completeness of the precipitation. If cloudiness appeared at the point of entry of the drop,

precipitation is not complete and further drops of $BaCl_2$ solution are added. The solution is kept at near boiling temperature for approximately 20 minutes (to give purer and larger crystals). Again further drops of $BaCl_2$ solution are added to check for complete precipitation.

4) The precipitate is filtered by pouring into a funnel that contained an ashless filter paper. Using distilled water, the precipitate is washed through, until the filtrate showed no chloride ion. The chloride ion test is carried out by placing few drops of $AgNO_3$ solution in a test tube and few drops of fresh washed from the funnel is allowed to fall into the test tube. A cloudy precipitate of AgCl shows that chloride ion is present. Washing continue until barely any cloudy precipitate appeared by chloride ion.
5) Using a crucible, the precipitated is dried in oven for 45 minutes at 110 ^oC. The amount of sulphate is calculated according to the calculations below.

Calculations

Mass of sample weighed, g (1)

Mass of filter Paper used, g (2)

Mass of filter Paper + dry precipitate, g (3)

Mass of dry precipitate = Mass of BaSO4 (4) = (3) – (2), g

Knowing the mass of BaSO4, it is possible to calculate the mass of sulphate in the sample according to Equation A4.1.

$$\text{Moles of } SO_4^{2-} = \text{Moles of } BaSO_4 = \frac{\text{grams of } BaSO_4}{\text{Molar mass of } BaSO_4}$$

Grams of SO_4^{2-} = moles of SO_4^{2-} x molar mass of SO_4

= grams of BaSO4 x $\frac{\text{molar mass of SO4}}{\text{molar mass of BaSO4}}$

% SO4 in sample = $\frac{\text{grams of SO4 in sample}}{\text{mass of sample in grams}}$ x 100

In order to determine the relative experimental error for this analysis, two trials are done on the highest initial ferrous concentration (R7). The calculations are shown below:

	Trial 1	Trial 2
Mass of sample weighed	0.3554 (g)	0.3541 (g)
Mass of filter Paper used	0.545 (g)	0.5302 (g)
Mass of filter Paper + dry precipitate	0.610 (g)	0.607 (g)
Mass of $BaSO_4$	0.065 (g)	0.0768 (g)
% SO_4 in sample	7.54	8.94

Average % of SO4 8.24

Relative error = [(8.24 - 7.54)/(8.24)]*100

= 8.5%

Appendix A5: Derivation of Mechanistic Rate Equation

Since the experimental data from this work is fitted to the rate equation proposed by Rönnholm *et al* (1999), it is necessary to summarise their derivation here for convenience. The non-catalytic rate equation is based on authors proposed oxidation mechanism (Chapter 1). These mechanisms are presented here again for convenience.

$Fe^{II} + O_2 = (Fe\text{-}O\text{-}O^*)^{2+}$ … (1)

$(Fe\text{-}O\text{-}O^*)^{2+} + Fe^{II+} = (Fe\text{-}O\text{-}O\text{-}Fe)^{4+}$ … (2)

$(Fe\text{-}O\text{-}O\text{-}Fe)^{4+} + Fe^{II+} = (Fe_2\text{-}O)^{4+} + (O\text{-}Fe)^{2+}$ … (3)

$(O\text{-}Fe)^{2+} + Fe^{II} = (Fe_2\text{-}O)^{4+}$ … (4)

$(Fe_2\text{-}O)^{4+} + H_3O^+ = OH^- + H_2O + 2\,Fe^{III}$ … (5)

$(H_3O)^+ + OH^- = 2H_2O$ … (6)

Overall reaction $4Fe^{2+} + O_2 + H_3O^+ = 6H_2O + 4Fe^{3+}$ … (7)

According to the authors, steps 1 and 2 are assumed to be the rate determining, such that:

… (8)

$$r = r1 = k_1[Fe^{II}][O_2] - k_{-1}[(Fe-O-O^*)^{2+}]$$
$$r = r2 = k_2[(Fe-O-O^*)^{2+}][Fe^{II}] - k_{-2}[(Fe-O-O-Fe)^{4+}]$$ … (9)

Assuming pseudo-steady-state hypothesis for intermediate $(Fe\text{-}O\text{-}O^*)^{2+}$, then r1=r2:

$$k_1[Fe^{II}][O_2] - k_{-1}[(Fe-O-O^*)^{2+}] = k_2[(Fe-O-O^*)^{2+}[Fe^{II}] - k_{-2}[(Fe-O-O-Fe)^{4+}]$$

Where

$$[(Fe-O-O^{*})^{2+}] = \frac{k_1[Fe^{II}][O_2] + k_{-2}[(Fe-O-O-Fe)^{4+}]}{k_2[Fe^{II}] + k_{-1}} \quad \ldots \quad (10)$$

Again, reactions 3 – 5 are assumed to be fast enough for quasi-equilibrium hypothesis to be applied. I.e. the net reactions is thus:

$$2Fe^{II} + (Fe\text{-}O\text{-}O\text{-}Fe)^{4+} + 4H_3O^{+} = 6H_2O + 4Fe^{III} \quad \ldots \quad (11)$$

Equilibrium constant is thus

$$K' = \frac{[Fe^{III}]^4[H_2O]^6}{[(Fe-O-O-Fe)^{4+}][Fe^{II}]^2[H_3O^{+}]^4} \quad \ldots \quad (12)$$

The intermediate concentration $(Fe\text{-}O\text{-}O\text{-}Fe)^{4+}$ is thus solved for as

$$[(Fe-O-O-Fe)^{4+}] = \frac{[Fe^{III}]^4[H_2O]^6}{K'[Fe^{II}]^2[H_3O+]^4} \quad \ldots \quad (13)$$

From (13), (10) and (8); the rate is expressed as:

$$r = k_1[Fe_{II}][O_2] - k_{-1}\left(\frac{k_1[Fe^{II}][O_2]}{(k_2[Fe^{II}] + k_{-1})} + \frac{k_{-2}}{(k_2[Fe^{II}] + k_{-1})} \cdot \frac{[Fe^{III}]^4[H_2O]^6}{K'[Fe^{II}]^2[H_3O^{+}]^4}\right) \quad \ldots \quad (14)$$

After denoting $K_1=k_1/k_{-1}$, $K_2=k_2/k_{-2}$ and overall equilibrium constant of Equation (7) as $Kc=K_1K_2K'$; Equation (14) is arranged in more practical form as:

$$r = \frac{k_2 K_1 [Fe^{II}]^2 [O_2]}{1 + (k_2 / k_{-1})[Fe^{II}]} \cdot (1 - q) \quad \ldots \quad (15)$$

Where

$$q = \frac{[Fe^{III}]^4 [H_2O]^6}{K_C [Fe^{II}]^4 [H_3O^+]^4} \quad \ldots \quad (16)$$

Two lamped parameters are introduced as $a_1 = k_2K_1 = \alpha\, e^{-E'1/RT}$ and $a_2 = k_1 = \beta\, e^{-E'2/RT}$ to reduced Equation (15) to

$$r = \frac{a_1 [Fe^{II}]^2 [O_2]}{1 + (a_1 / a_2)[Fe^{II}]} \cdot (1 - q) \quad \ldots \quad (17)$$

From Equation (16), if Kc is large, $q \rightarrow 0$; and to avoid overparameterisation, the ratio a_1/a_2 is assumed to be independent of temperature. Activation energy is then introduced and Equation (17) becomes:

$$r = \frac{\alpha [Fe^{II}]^2 [O_2]}{1 + (\alpha / \beta)[Fe^{II}]} \cdot e^{-E/RT} \quad \ldots \quad (18)$$

The form of rate expression used for the data fitting.

Appendix A6: More on Fitted Data

The following are more on the fitted experimental data for different starting ferrous concentrations, temperature and type of oxidant used.

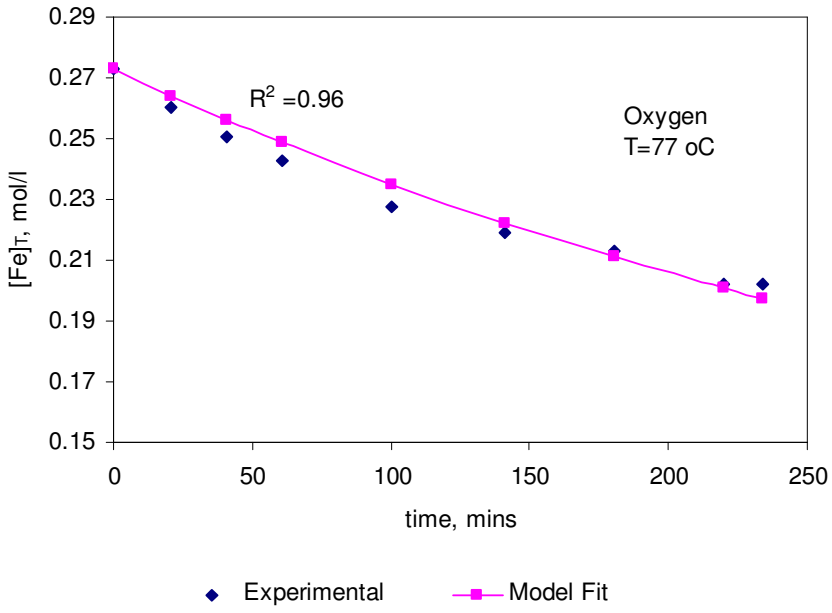

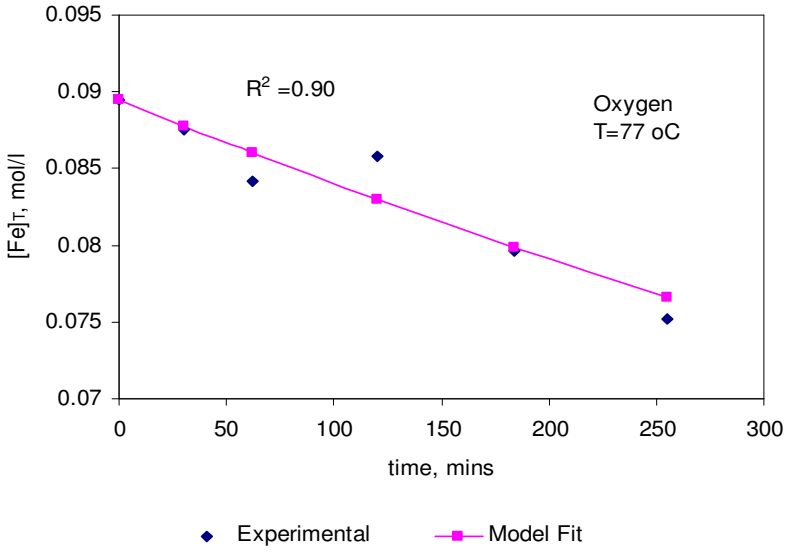

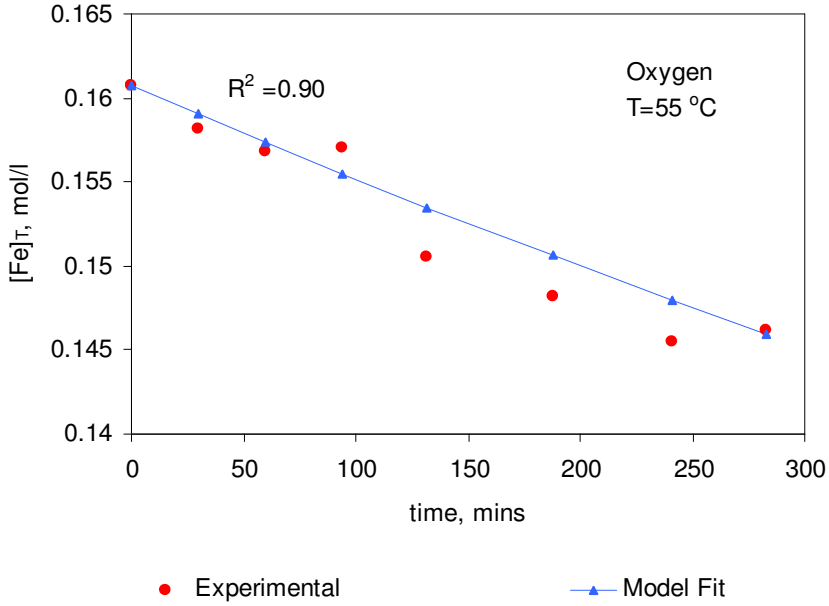

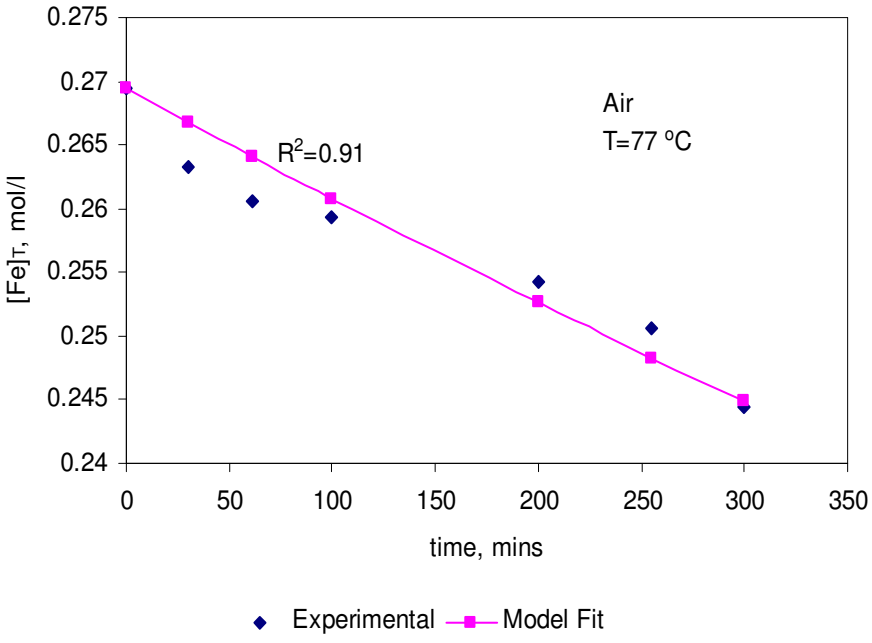

Figure A6.1 Comparison of model with Experiment Cont.

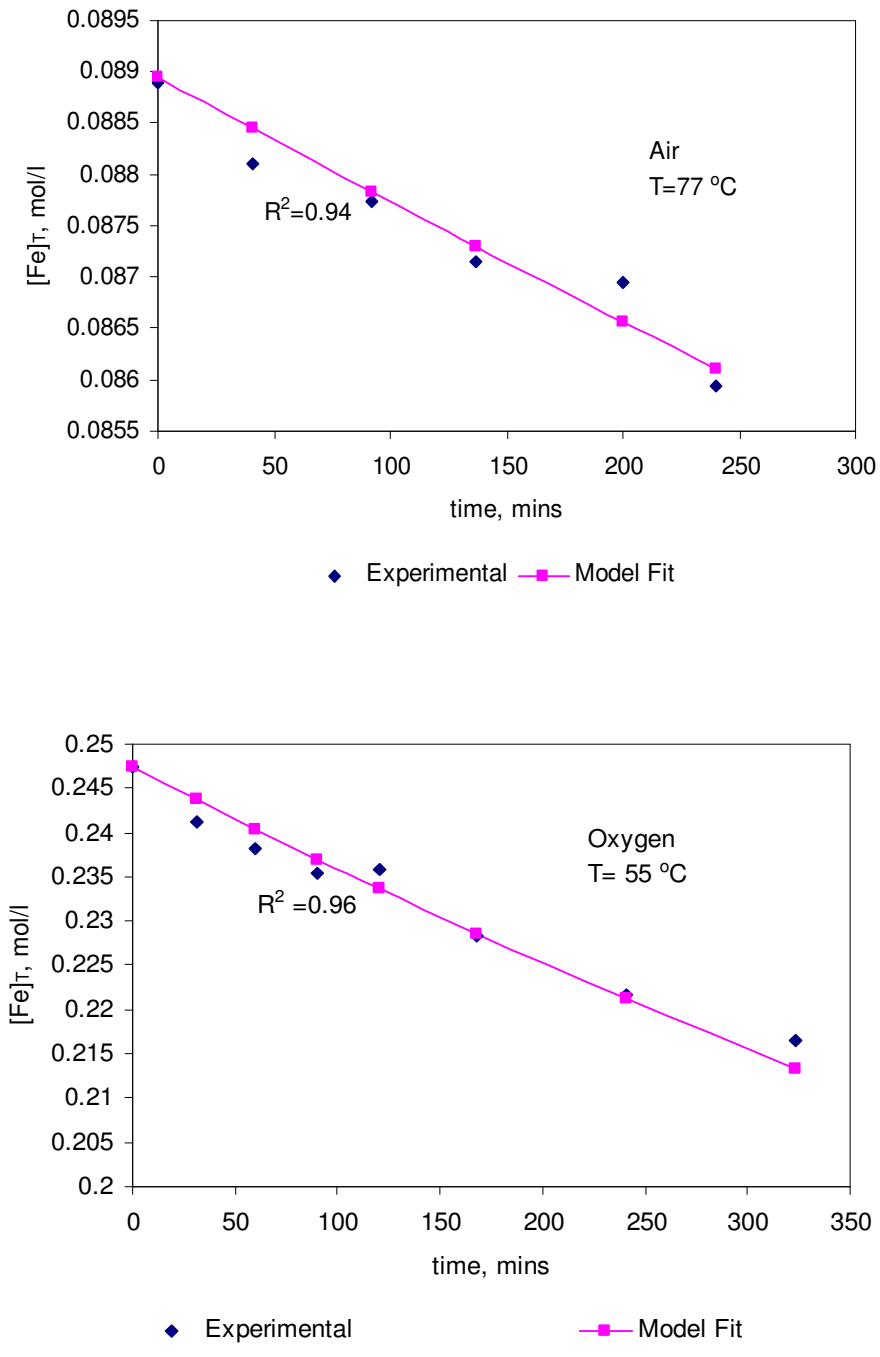

Figure A6.1 Comparison of model with experimental Data Cont.

Appendix A7: Program For Non-Linear Regression Modelling

The program for the estimation of the parameters is quite long to include them all, therefore sample of it is presented here as an illustration.

Experimenta Data

$C_{Fexp} := (0.345341 \quad 0.331543 \quad 0.318225644 \quad 0.308615 \quad 0.276861 \quad 0.267861 \quad 0.252662 \quad 0.243984 \quad 0.240029)^T$

$t := (0 \quad 21.0833 \quad 43 \quad 60 \quad 127 \quad 151 \quad 203 \quad 250 \quad 300)^T$

parameters to be estimated

$A_1 := 5.4 \cdot 10^9 \qquad A_2 := 9.0 \cdot 10^9 \qquad E := 58900$

$R := 8.314 \qquad T := (273 + 77)$

$\frac{A_1}{A_2} = 0.6$

starting ferrous concn .

saturated oxygen concn

$C_{Feo} := 0.345341 \qquad C_{O2} := 0.00070386$

$\frac{E}{8.314} = 7.084 \cdot 10^3$

$C_{Fe} := 0.3$

Given

$$\frac{1}{C_{Fe}} - \frac{A_1}{A_2} \cdot \ln\left(C_{Fe}\right) = \frac{1}{C_{Feo}} - \frac{A_1}{A_2} \cdot \ln\left(C_{Feo}\right) + A_1 \cdot C_{O2} \cdot \exp\left(\frac{-E}{R \cdot T}\right) \cdot t$$

$C_{Fe}(A_1, A_2, t) := \text{Minerr}(C_{Fe})$

Calculates the ferrous concentrations for the given parametrs

$n := 0 .. 8$

$C_{Fe_n} := C_{Fe}(A_1, A_2, t_n)$

calculates the sum of residual square error by comparing the experimental and calculated values of the ferrous concns.

$SSE1 := \sum_n \left(C_{Fexp_n} - C_{Fe_n}\right)^2$

$SSE1 = 3.804 \cdot 10^{-4}$

$C_{Fe_n} =$

0.345341
0.3329430152
0.3208938913
0.312087339
0.2813428543
0.2716591518
0.2526740536
0.2375364964
0.2232006897